Shallow and deep subsurface sediment remobilization and intrusion in the Middle Jurassic to Lower Cretaceous Agardhfjellet Formation (Svalbard)

Kei Ogata[1,2], Annelotte Weert[1,2], Peter Betlem[3,4], Thomas Birchall[3,4], and Kim Senger[3]

[1]Department of Earth and Life Sciences, Geology and Geochemistry Cluster, Vrije Universiteit (VU) Amsterdam, De Boelelaan 1085, 1081 HV Amsterdam, The Netherlands
[2]Dipartimento di Scienze della Terra, dell'Ambiente e delle Risorse (DiSTAR), Università degli Studi di Napoli "Federico II," Complesso Universitario Monte S. Angelo, Edificio L, Via Vicinale Cupa Cintia 21, 80126 Napoli, Italy
[3]Department of Arctic Geology, The University Centre in Svalbard, P.O. Box 156, 9171 Longyearbyen, Norway
[4]Department of Geosciences, University of Oslo, Sem Sælands vei 1, 0371 Oslo, Norway

ABSTRACT

Sedimentary injectites are increasingly documented in many hydrocarbon plays at various scales, either interpreted as potential risks (e.g., top-seal bypass, a drilling hazard) or benefits (e.g., reservoir interconnection, increased hydrocarbon volumes) for production operations. As such, they have potential critical implications for the assessment of suitability for CO_2 injection and sequestration. Detailed characterization of such units, especially in terms of diagenesis and (paleo) fluid flow, is directly achievable at outcrop scale, overcoming dimensional and time constraints otherwise unresolvable at seismic scale.

Two sedimentary injection complexes have been recognized in the succession of the Middle Jurassic–Lower Cretaceous Agardhfjellet Formation exposed at Deltaneset, central Spitsbergen, Norway, at different stratigraphic levels. The upper complex comprises two main clastic dikes characterized by different orientation and consolidation, tapering out vertically (upward and downward) within a stratigraphic thickness and lateral extent of more than 50 m and 200 m, respectively. The lower complex is coarser grained, made up by a network of interconnected dikes and sills, shooting off from isolated lenticular and morphologically articulated bodies, interpreted as sedimentary intrusions linked to seafloor extrusion (sand volcano). Petrographic and micromorphological analyses were used to identify the underlying lithologies of the Late Triassic to Middle Jurassic Wilhelmøya Subgroup as the possible source of this remobilized material for both the upper and lower complexes. This subsurface remobilization and consequent intrusion were first achieved in the lower complex during the Late Jurassic at shallow burial conditions, and then at higher confinement pressure for the upper complex, probably during the Late Cretaceous. These results highlight how field data can be used to constrain long-lived spatiotemporal relationships of sedimentary intrusions, allowing a finely tuned upscaling of seismic data and interpretations.

■ INTRODUCTION

The increasing importance of sedimentary injections in the exploration and exploitation of the shallow and deep subsurface has been proven in recent years, along with their role within reservoir-seal systems (Grippa et al., 2019; Bradaric et al., 2022). Nonetheless, most of this knowledge comes from large-scale sandstone intrusion complexes observed in seismic profiles and cubes (Grippa et al., 2019), and there is a general paucity of detailed data collected at finer scales, such as those coming from outcrop-based studies (e.g., Jolly and Lonergan, 2002; Hurst et al., 2011; Cobain et al., 2015, 2017; Cobain, 2016).

Here, we analyzed two field occurrences from the Late Jurassic Agardhfjellet Formation exhumed in central Spitsbergen, Svalbard, Norway. This 220-m-thick succession of organic-rich shales, besides being a renowned regional source rock in the Barents Shelf, also represents an ideal cap rock for potential geological storage of carbon dioxide, as documented by the Longyearbyen CO_2 Laboratory project (Braathen et al., 2012; Olaussen et al., 2019). This project envisioned an onshore, pilot-scale site for CO_2 injection in a Late Triassic reservoir rock at 700–1000 m depth below the settlement of Longyearbyen (Braathen et al., 2012), and the research presented here represents a follow up of the baseline structural-stratigraphic investigations carried out on the exhumed part of this target succession (Ogata et al., 2014).

Mesoscale sedimentary intrusions (centimeter- to meter-sized sandstone dikes) in this unit have been documented since the 1980s and at first were assumed to be related to passive injection during the Paleogene (Wierzbowski and Ziembińska-Tworzydło, 1984). More recent studies argued for active injection much earlier, resulting from an overpressured source rock located somewhere below the Agardhfjellet Formation (Hammer and Nakrem, 2010; Ogata et al., 2014). Additionally, it was also suggested that the sedimentary intrusions may represent a plumbing system for the methane seeps found in the same area (Hammer et al., 2011).

In this framework, understanding the occurrence of such sedimentary injectite systems in the

K. Ogata https://orcid.org/0000-0002-4978-2854

Agardhfjellet Formation will provide clues about their possible role in underground gas storage, for instance, as seal bypass systems or reservoir connectors. Moreover, characterizing their emplacement mechanisms and testing their significance as paleo-tectonic indicators will thus provide useful insights on their influence on subsurface fluid flow in shale-dominated lithologies.

Accordingly, this study aimed to provide a detailed qualitative and quantitative structural-stratigraphic characterization of these sedimentary intrusions, supported by extensive micromorpho-logical and petrographic analysis.

■ GEOLOGICAL OUTLINE

The Svalbard archipelago represents the uplifted part of the northwest margin of the Barents Shelf (Fig. 1A; Harland, 1997b). The geological evolution is marked by northward drifting, from equatorial lat-itudes in the Paleozoic to the polar latitudes of today (Worsley, 2008). During its drift north, Svalbard expe-rienced the Caledonian orogeny and older events, erosion and extension in the Devonian, contraction by the end of the Devonian, localized rifting in the Carboniferous, Permian to Mesozoic stable platform conditions with long-term sedimentation, and mafic dike and sill intrusion during the Late Cretaceous, eventually establishing as a transform plate margin during the Cenozoic (e.g., Harland, 1997a; Dallmann, 2015). Opening of the Atlantic Ocean during the Paleo-gene caused dextral movement along the Hornsund fault zone (Fig. 1B), rifting Svalbard and Greenland apart (Eldholm et al., 1987; Braathen et al., 1995; Faleide et al., 2008; Leever et al., 2011). Consequently, oblique compression led to the development of the West Spitsbergen fold-and-thrust belt and Paleo-gene Central Spitsbergen Basin (Steel et al., 1985; Braathen et al., 1995; Harland et al., 1997a; Helland-Hansen, 2010).

Our study area, located at Deltaneset, is posi-tioned on the northeastern margin of the Central Spitsbergen Basin (Fig. 1C). The area includes a Mesozoic sedimentary succession with brittle frac-turing, likely the result of compression and related folding associated with the West Spitsbergen

fold-and-thrust belt (Bergh et al., 1997). The tar-geted strata are the Late Jurassic Agardhfjellet Formation, bordered by the Early Cretaceous Rurikfjellet Formation on top and Middle Jurassic Wilhelmøya Subgroup below (Fig. 1D; Mulrooney et al., 2019). These target deposits record a shallow-marine shelf to prodeltaic setting (Dypvik et al., 1991) under dysoxic to anoxic conditions with peri-odic oxygenation of the bottom water (Collignon and Hammer, 2012).

The Agardhfjellet Formation is divided into four members (Fig. 2): the lowermost Oppdalen Mem-ber, succeeded by the Lardyfjellet and Oppdalssåta Members, and the Slottsmøya Member on top (Dypvik et al., 1991; Koevoets et al., 2019). All four members are exposed in the study area, with a combined thickness of 220 m (Koevoets et al., 2016).

■ METHODS

Data were collected from two areas, in the northeastern side of Janusfjellet (Wierzbowski and Ziembińska-Tworzydło, 1984; Hammer and Nakrem, 2010) and the northwestern side of Konusdalen (Ogata et al., 2014) (see Figs. 1D and 2). Systematic sampling of the injectite material from surficial and surrounding country beds was performed, along with high-resolution mapping (1:100 scale) and structural-stratigraphic logging. Mesoscale structural data such as reference bedding, orientation of single injectite branches, local thickness, and orientation of internal and external structures were collected in situ along with dedicated, high-resolution photogram-metric acquisition, both ground- and unmanned aerial vehicle (UAV)–based. The resultant digital outcrop models (DOMs) and high-resolution aerial orthophotos (https://data.npolar.no/dataset/66a42347 -036e-472a-bc93-67c1a5c3e1d2) were used to com-plement the field-based analyses. Due to the poor environmental conditions during ground-based pho-togrammetric acquisition, the obtained DOMs were only used to obtain qualitative data.

In total, 41 samples were taken, representing in situ material from the injectites' filling, host-rock material, and unoriented injectite material from surficial, weathered parts of outcrops. The samples

from the country rock and injectite material (mar-gins and interior) were systematically collected to outline diagnostic geochemical and structural markers, in order to identify the source rock and characterize the anatomy of the injectites. Specific samples for comparison were also collected from the overburden and underburden formations (Car-olinefjellet Formation, Rurikfjellet Formation, and Wilhelmøya Subgroup, respectively).

Thin-section petrography, scanning electron microscopy (SEM), and energy-dispersive X-ray spectroscopy (EDS) were used in combination for mineralogical, microstructural, micromorphological, and sedimentological characterization of a total of 54 thin sections. The bulk sample composition was derived by studying the mineralogy, size, spheric-ity, and roundness of over 100 random grains in each thin section. Clasts, matrix, and cement com-positions were also studied for mineralogical and petrographic fingerprinting. Analysis with EDS was used to identify chemical differences between tex-tural components within samples.

■ DATA AND RESULTS

The investigated sedimentary intrusions occur at two different stratigraphic levels: the upper complex located on the NE side of Janusfjellet, just below the lower boundary of the Rurikfjellet Formation, and the lower complex located on the NW side of Konusdalen, ~20–30 m above the top of the Wilhelmøya Subgroup (see Figs. 1D and 2). They crop out as positive topographic features, cut-ting through the black shales of the Agardhfjellet Formation, but not continuing in the deposits of the overlying Rurikfjellet Formation and underlying Wilhelmøya Subgroup.

The overall composition of all injectites is similar, composed of fine- to medium-grained sandstone with silty shale and rounded lithic clasts. Subverti-cal dikes and subhorizontal sills mainly characterize the upper complex and lower complex, respectively. Isolated mounds, characterized by higher lithifica-tion and contrastingly light-yellow alteration color (Figs. 3A and 3B) compared to the typical surround-ing black shales (Figs. 3C and 3D) of the Slottsmøya
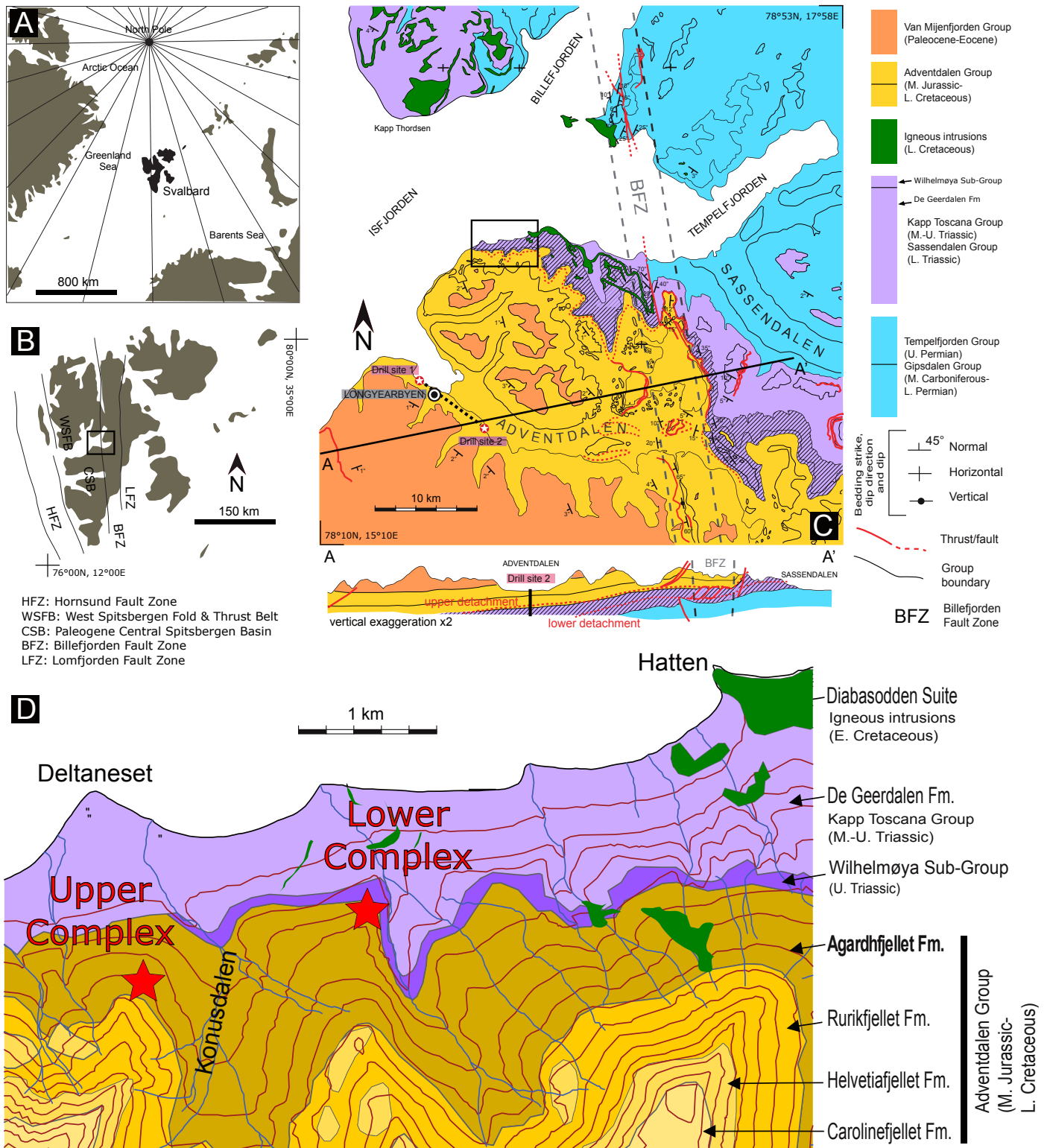
Figure 1. Geographic and geologic setting. (A) Location of the Svalbard archipelago. (B) Main regional tectonic features of Svalbard. (C) Simplified geological map and cross section of the inner Isfjorden area. (D) Geological map of the investigated area. Figure is modified from Ogata et al. (2014).
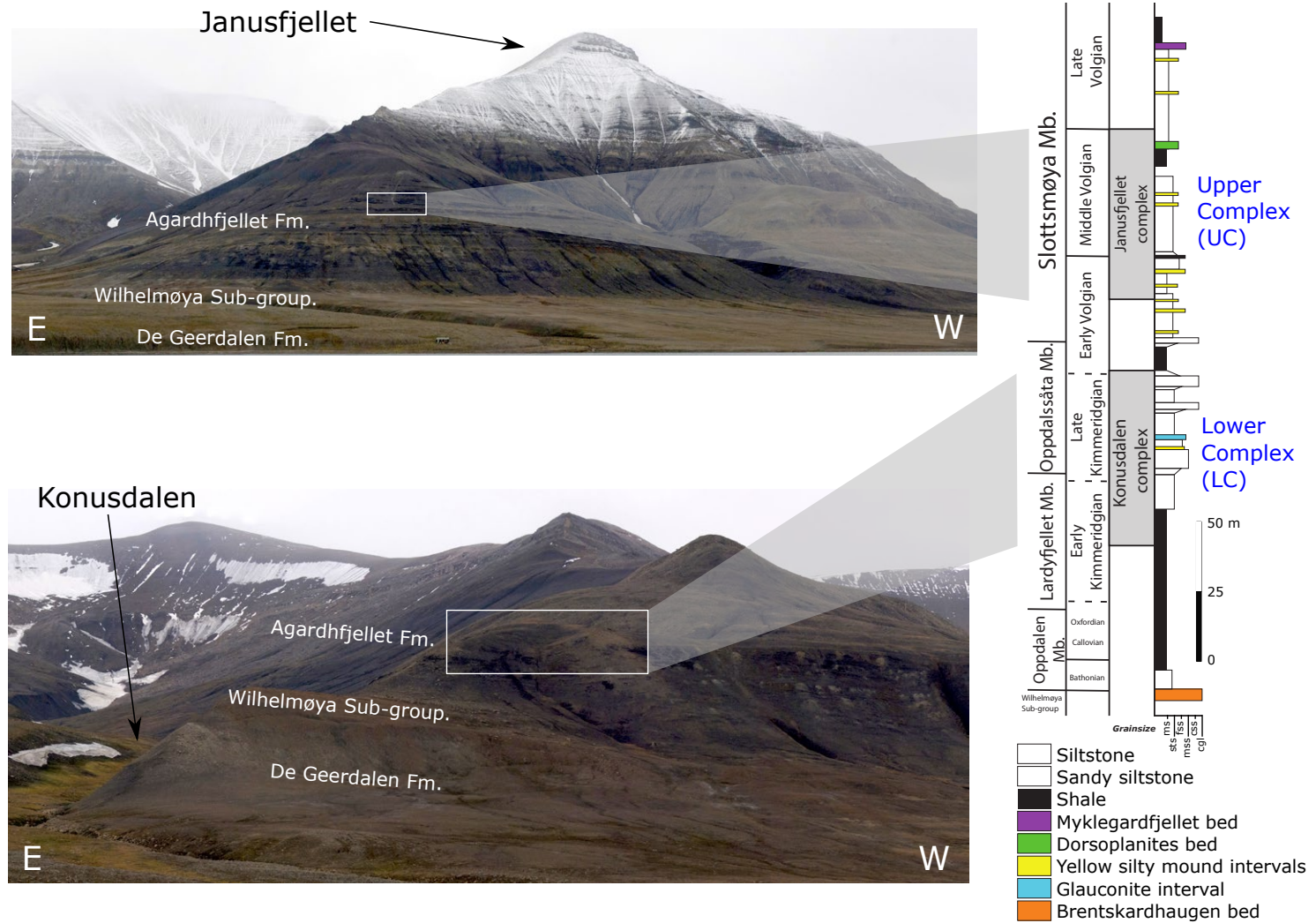
Figure 2. Panoramic pictures of the two investigated areas, with indication of their stratigraphic position within the Middle–Late Jurassic sedimentary succession (modified from Koevoets et al., 2016). Grain size: ms—mudstone; sts—siltstone; fss—fine sandstone; mss—medium sandstone; css—coarse sandstone; cgl—conglomerate.
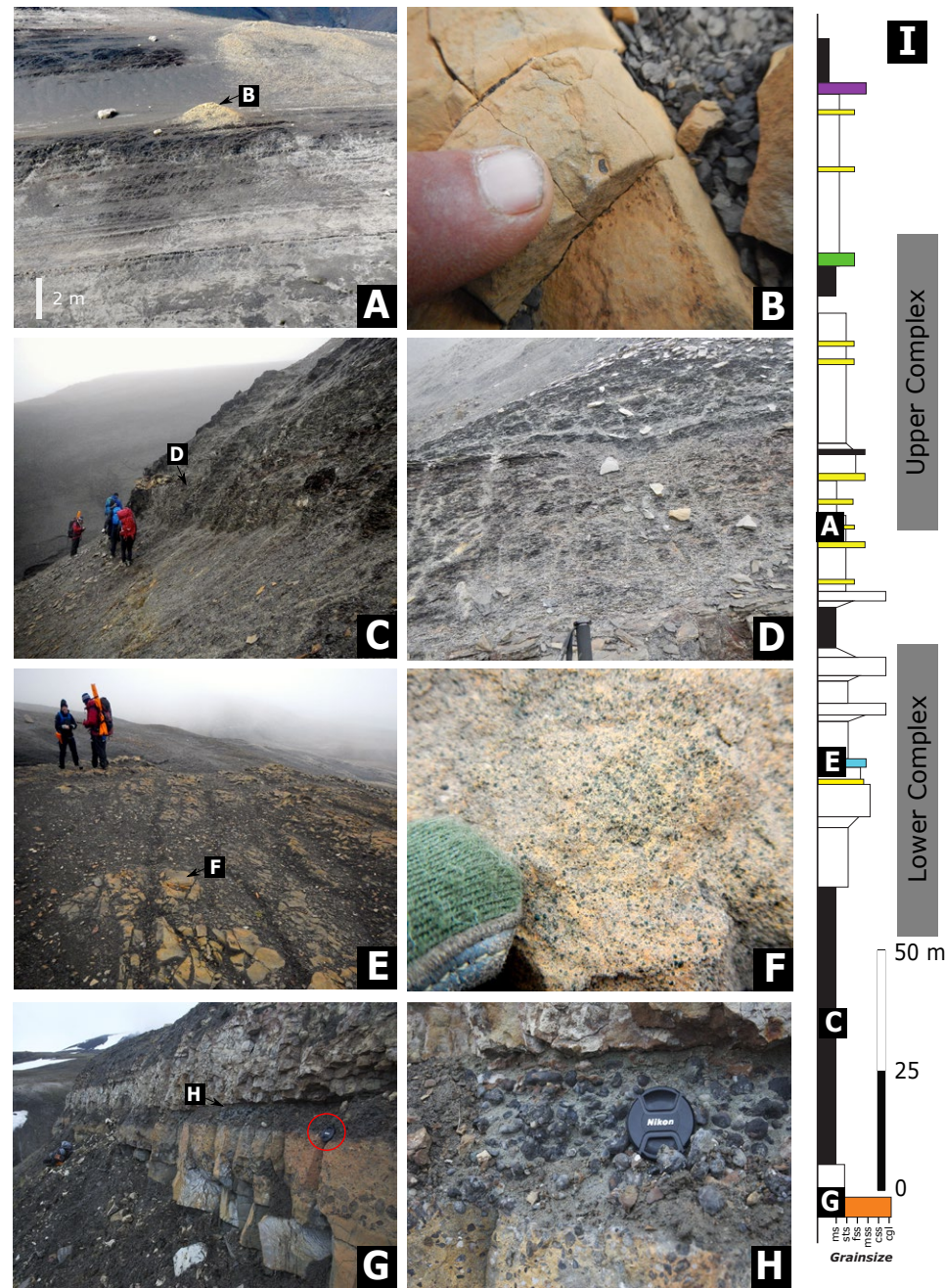
Figure 3. Details of the host-rock formations. (A) Silty mound embedded in the Agardh-fjellet Formation shales, the alignment of which defines a marker stratigraphic interval. (B) Detail of A showing a millimeter-sized rounded pebble enclosed within the silty mound. (C) Organic shale interval of the Agardhfjellet Formation. Note an iso-lated yellow silty lens on the left side of the outcrop. (D) Detail of C showing the typical foliated appearance of the silty, organic-rich paper shales. (E) Fossilifer-ous, coarse-grained glauconitic sandstone making up the Glauconite marker interval in the Oppdalssåta Member. (F) Detail of E showing millimeter-sized glauconitic flakes. (G) Composite, conglomeratic Brentskard-haugen Bed of the Wilhelmøya Subgroup, which is a regional condensed section and stratigraphic marker. (H) Detail of G showing an unconsolidated part of the conglomer-ate interval systematically occurring in the middle of the unit, made up mainly by centimeter-sized, rounded phosphatic peb-bles. (I) Stratigraphic log of Figure 2 with locations of the illustrated lithologies. Grain size: ms—mudstone; sts—siltstone; fss—fine sandstone; mss—medium sandstone; css—coarse sandstone; cgl—conglomerate.

Ogata et al. | Sediment intrusions in the Agardhfjellet Formation (Svalbard)

and Oppdalssåta Members of the Agardhfjellet Formation, are found around both injectite complexes.

In particular, the lower complex builds up within a coarsening- and thickening-upward succession in the upper part of the Oppdalssåta Member, characterized by competent, fossiliferous, glauconite-rich siltstones and sandstones (Figs. 3E and 3F). The top of the Wilhelmøya Subgroup crops out ~50 m below this interval, and it is represented by the regional Brentskardhaugen Bed, a lithologically mature, composite arenaceous-conglomeratic bedset with a thickness of ~2–3 m (Fig. 3G). This bedset is made up of intervals of orthoconglomerates and paraconglomerates with a coarse, quartz-rich sandstone matrix containing rounded pebbles and phosphatic nodules up to several centimeters in size. It displays variable cementation and is unconsolidated in the middle part (Fig. 3H).

Sample locations, SEM/EDS, petrographic, and mineralogical data along with micromorphological and DOM data are provided in the Supplemental Material.[1]

Upper Complex

Two distinct sedimentary dikes were identified within the upper complex, located within the Slottsmøya Member on the northeastern side of Janusfjellet (see Fig. 2). One dike had already been reported before by Wierzbowski and Ziembińska-Tworzydło (1984) and Hammer and Nakrem (2010). The dikes are vertically oriented and roughly tabular-shaped, with widths varying between 10 cm and 40 cm, and they are traceable up to 200 m (Fig. 4). Both dikes are arranged at high angle with respect to the nearly horizontal background stratification, and apart from one normal fault oriented approximately ESE-WNW, with few meters of oblique displacement, no major structural lineaments were observed (see Fig. 4).

The dikes have a similar composition, consisting of unsorted, poorly consolidated, fine- to medium-grained sandstone (Figs. 5A–5C). This includes rounded quartz, lithic grains (up to 1 cm), and angular silty shale clasts with the same characteristics as the surrounding shales of the host rock (Figs. 5D–5G). The dikes have two main orientations, striking NE-SW (N50°) and E-W (N85°), with dip angle varying from subvertical to 30° as the lowest value (Fig. 6A), and they show a maximum and minimum thickness variation from 70 cm to 20 cm, respectively. The former shows a sharp kink in the upper part (toward the S), where it becomes E-W–oriented, subparallel to the direction of the other one, and wedging out across the *Dorsoplanites* bed (Fig. 6E).

The dikes have a relatively straight geometry, with some kinks and sinistral offsets due to layer-parallel shear surfaces and polished slickensides oriented approximately ESE-WNW (N190° to N210°) and horizontal displacements up to 1 m, crosscutting the dikes and making them appear segmented (Fig. 6F).

The lateral and vertical terminations of the dikes are characterized by relatively abrupt tapering/wedging, showing variable lithological contrast with the surrounding black shales. In fact, the consolidation of the injectites' interior varies, being well consolidated in the upper-middle parts of the exposure and becoming poorly to unconsolidated downward, requiring excavation to trace them (Fig. 6G).

When well consolidated, their lateral margins appear to be sharp, relatively smooth, and flat, with evidence of linear structures such as parallel ridges with hackle marks. Internally, they are massive and unsorted, showing a localization of angular, centimeter-sized mudstone clasts at the sides. Other structures observable on the outer-wall surfaces are crude, mullion-like, millimeter-scale corrugations, arranged as subparallel ridges on the surfaces. The ridges are aligned parallel to the dike margins and subparallel to the bedding plane (Figs. 6H–6I).

Lower Complex

At least two sills and four dikes were identified within the lower complex at Konusdalen (see

Fig. 2), forming a network of relatively thin (up to 10 cm) clastic intrusions, apparently radially oriented from a discrete, mounded coarse sandstone body ~50 m in diameter (Fig. 7). The injectites have thicknesses varying from 5 cm to 80 cm, are traceable up to 10 m laterally, and seem to be bounded at the top by a glauconite marker interval of the Oppdalssåta Member.

The area appears to be crosscut by at least two sets of structural lineaments oriented NW-SE and NNE-SSW, which appear to be locally confined within the lower part of the Agardhfjellet Formation (see Fig. 7). These structures do not show appreciable displacement and mutual crosscutting relationships, with the NW-SE set apparently abutting against the NNE-SSW set.

The injectites are composed of a clast-supported, fine- to coarse-grained, pebbly sandstone with rounded quartz and lithic grains (up to 4 cm) characterized by a distinctive reddish oxidation color (Figs. 8A–8C). Microscopically, these pebbly sandstones appear to be texturally and compositionally mature with very well-rounded and highly spherical quartz grains and phosphate/dolomite nodules embedded in a fine-grained, ferroan-calcite cement (Figs. 8D–8E). The overall grain size seems to increase toward the isolated sandstone body.

The dikes show three main sets of orientation: NE-SW (N34°), NNW-SSE (N154°), and ENE-WSW (N80°), appearing to be connected by sills (Fig. 9A). The black shales around coarse-grained, pipe-shaped injections found ~3–4 m underneath the mounded sandstone body show strikingly red to yellow oxidation colors (Figs. 9B–9C).

The mounded, coarse sandstone body is located at the SSE end of the lower complex, appearing as a convex positive structure. It has a flat cone-like shape and is composed of a fine-grained conglomerate with quartz grains and lithic clasts (up to 0.5 cm), which get coarser in the center of the structure (Fig. 9D). The injectite network seems to be radially oriented with respect to this structure.

The sills appear in segments, separated by normal offsets of a few centimeters. The top margins of the sills are smooth, with remnants of the black shale of the host rock as clay smear on top (Fig. 9E). Both dike and sill structures are distributed at
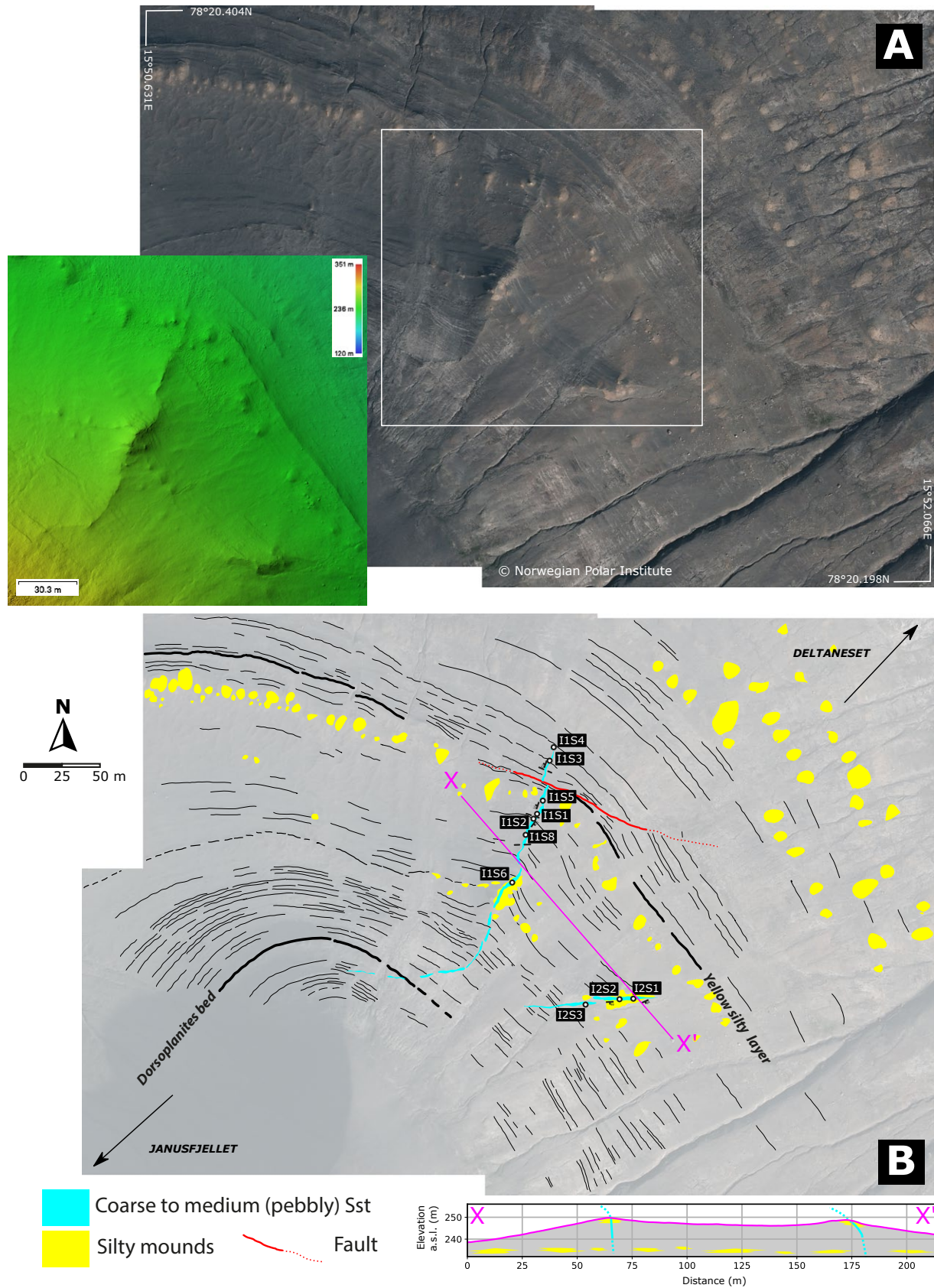
Figure 4. (A) Aerial photograph (courtesy of the Norwegian Polar Institute) and (B) ground-truthed interpretation of the upper complex (UC) at Janusfjellet, Svalbard, Norway. Digital elevation model (DEM; inset in A) and interpreted cross section (in B) are also provided. Location is shown in Figures 1D and 2. Positions of samples are labeled. Sst—sandstone.
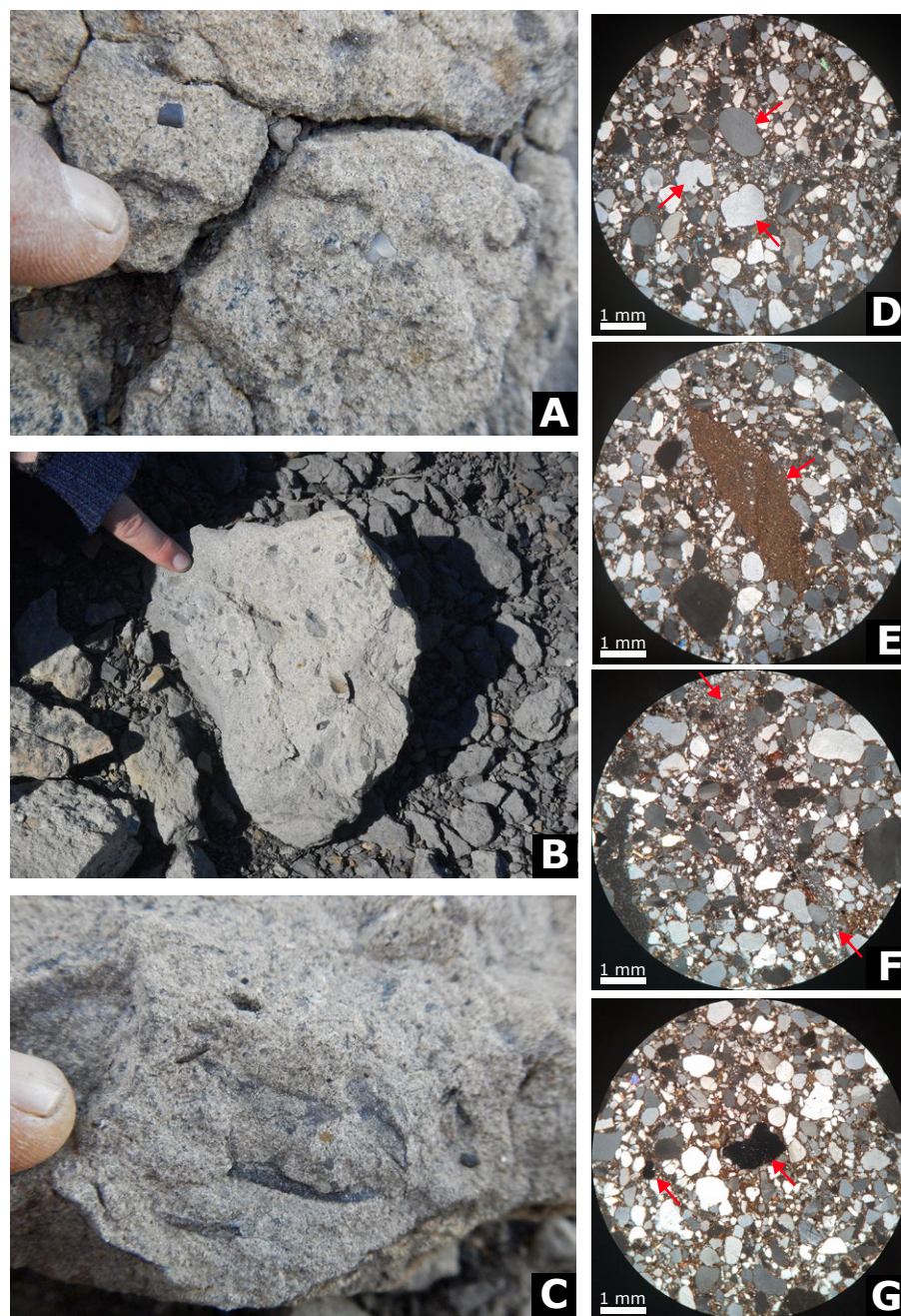
Figure 5. Mesoscopic and microscopic appearance of the injectite material making up the dikes of the upper complex. (A) Pebbly sandstone making up the upper part of dike 1, upper complex. Note the subrounded, crystalline clasts. (B) Coarse sandstone with angular shale intraclasts making up the intermediate part of dike 1. (C) Coarse sandstone with angular shale intraclasts and organic material making up dike 2. (D) Microphotograph of the middle–lower part of dike 1 showing the abundance of rounded and spherical quartz clasts, some of which show corroded rims (sample I1S1). (E) Microphotograph of the middle–lower part of dike 1 showing an angular siltstone intraclast (sample I1S1). (F) Microphotograph of the middle–lower part of dike 1 showing a disaggregation deformation band (sample I25). (G) Microphotograph of the middle part of dike 2 showing organic fragments (sample I2S2).

different stratigraphic levels, across an interval of ~50 m, and are characterized by complex internal features (e.g., particle banding, intrafolial folding, fluidal structures) and kinks and sharp boundaries with the country rock (Fig. 9F). Some dikes also show mud clasts (up to 10 cm) in the top segment (Fig. 9G). These clasts show the same lithology as the wall rock, being most likely detached from it, and the fissures are filled by injectite material. Within the dikes, grading is present, with an increasing grain size toward the center of the injectite. Mullion-like, soft-sediment corrugations and striations similar to those identified in the upper complex were also observed in some of the dike margins (Fig. 9H).

Close to the lower boundary with the black shale interval capping the Wilhelmøya Subgroup, isolated outcrops of massive coarse sandstones occur over a stretch of a few tens of meters, arranged in a 2–3-m-thick, elongated body resembling a composite, segmented sill network linked by inclined oversteps (see Fig. 9F) and centimeter-thick dikes (Fig. 9I). Such sandstones show marked differential consolidation at the outcrop scale, being characterized by a high content of shaly intraclasts (see Fig. 9G).

Associated with these sandstones, there are isolated, conglomeratic bodies ~20 m across that appear to be completely enclosed within the black shales of the lower Agardhfjellet Formation (Fig. 9J). These conglomerates are made up by subrounded

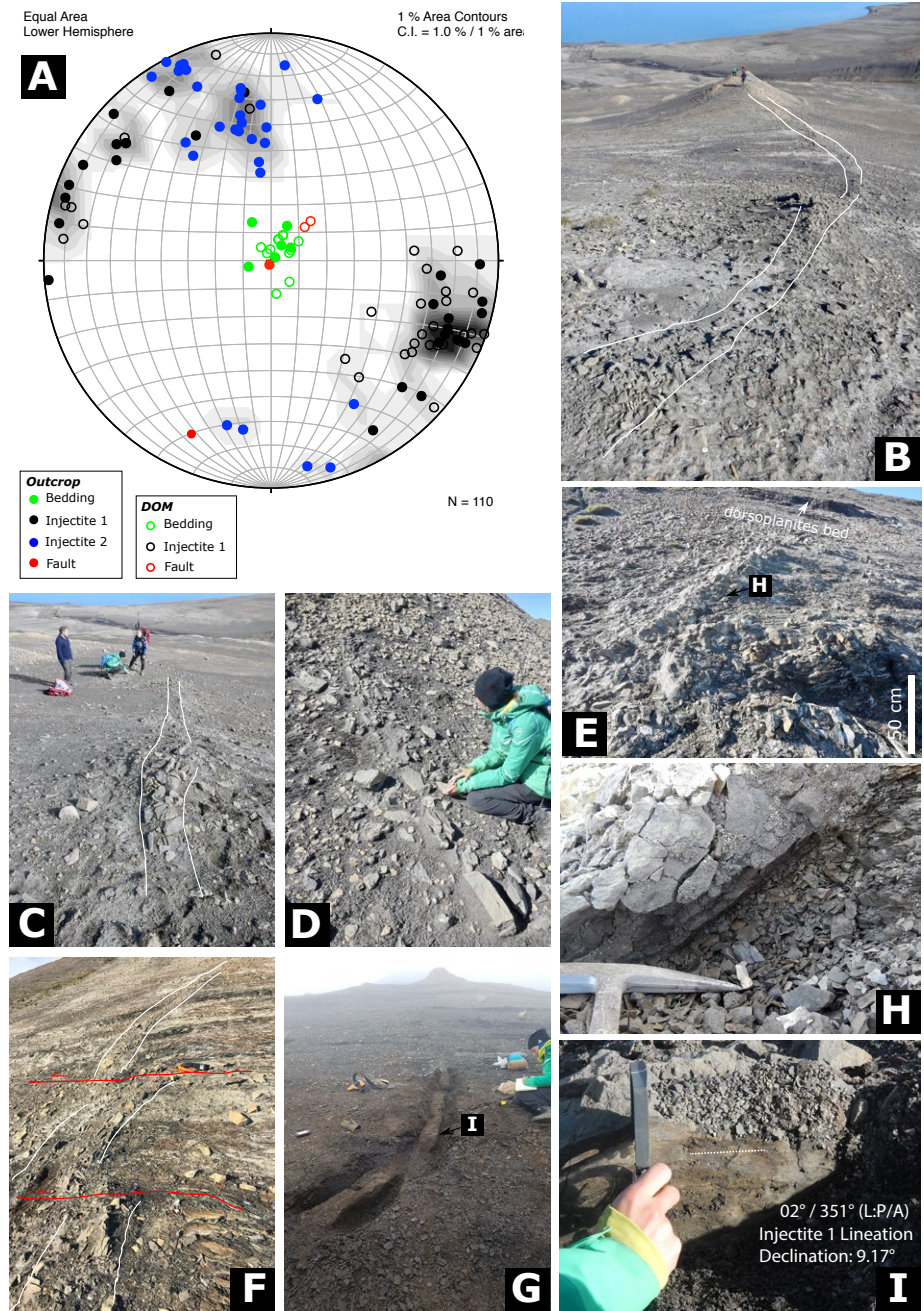Ogata et al. | Sediment intrusions in the Agardhfjellet Formation (Svalbard)

Figure 6. Outcrop appearance and spatial distribution of the dikes forming the upper complex. (A) Stereoplot of structural-stratigraphic data from field work and digital outcrop model (DOM) analysis summarizing the injectite structures comprising the upper complex. (B) Middle part of dike 1 showing the bending toward the W. (C) Lower part of dike 2, characterized by low relief. (D) Upward termination and wedging out of dike 2. (E) Upward termination and wedging out of dike 1 toward the *Dorsoplanites* bed. Note also the change in inclination from nearly vertical to ~50°. (F) Bedding-parallel striated and polished surfaces cross-cutting the middle part of dike 1 with tens of centimeters of offset. (G) Lowermost part of dike 1, which appears to be unconsolidated with no erosional relief. (H) Detail of the sharp inclined contact of dike 1 with the surrounding paper shapes as shown in part E. (I) Detail (and spatial attitude) of the lineations observed on the sides of dike 1 as shown in part G. L:P/A refers to lineation:plunge/azimuth.

clasts up to several centimeters in size, mostly composed of phosphate nodules. The appearance is generally matrix-supported, appearing unconsolidated to poorly consolidated, which provides the low topographic relief (Figs. 9K–9L).

Micromorphology and Structural Diagenesis

At microscale, the dikes from the upper complex include subrounded to well-rounded, poorly sorted grains in a very fine-grained matrix (see Fig. 5). The matrix is a detrital mixture of quartz and aluminosilicates (<0.1 mm), with 75% of the grain-size population ranging between 0.1 mm and 1 cm (Fig. 10). The roundness of the grains ranges between 0.5 and 0.9, with an average of 0.7. The sphericity yields values between 0.7 and 0.9 (Fig. 11A).

Toward the margins of the dikes, grain-size reduction and increased packing were observed. Along the margins, secondary clay minerals, like sheet aluminosilicates and glauconite, appear. The composition of the grains is dominated by quartz (~60% of total mineral content), appearing in different forms; most of the quartz grains are monocrystalline, but polycrystalline quartz, chalcedony, and chert were identified as well, with 60% showing undulose extinction. Other identified
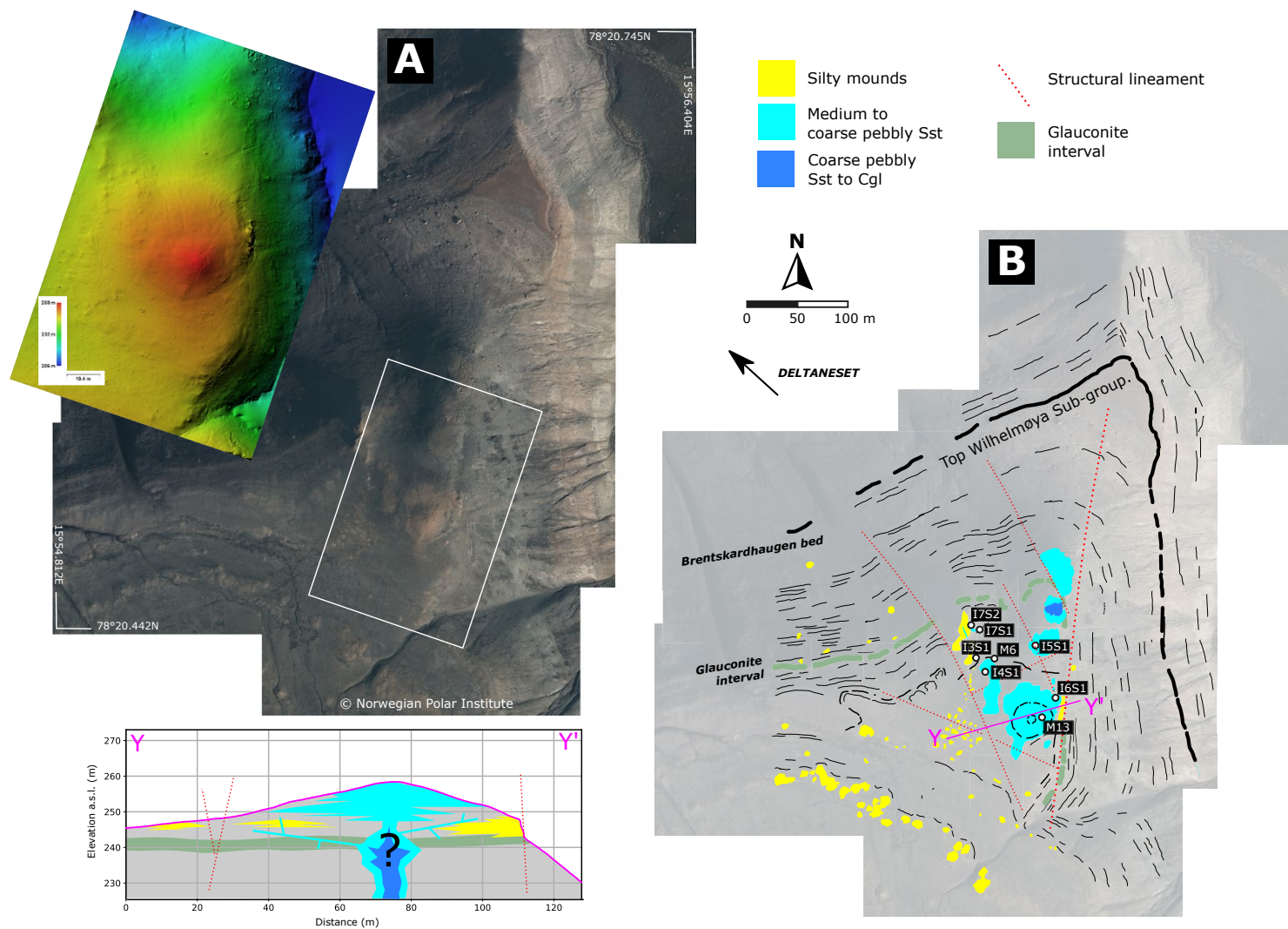
Figure 7. (A) Aerial photograph (courtesy of the Norwegian Polar Institute) and (B) ground-truthed interpretation of the lower complex (LC) at Konusdalen. Digital elevation model (DEM; inset in A) and interpreted cross section (in B) are also provided. Location is shown in Figures 1D and 2. Positions of samples are labeled. Sst—sandstone; Cgl—conglomerate.
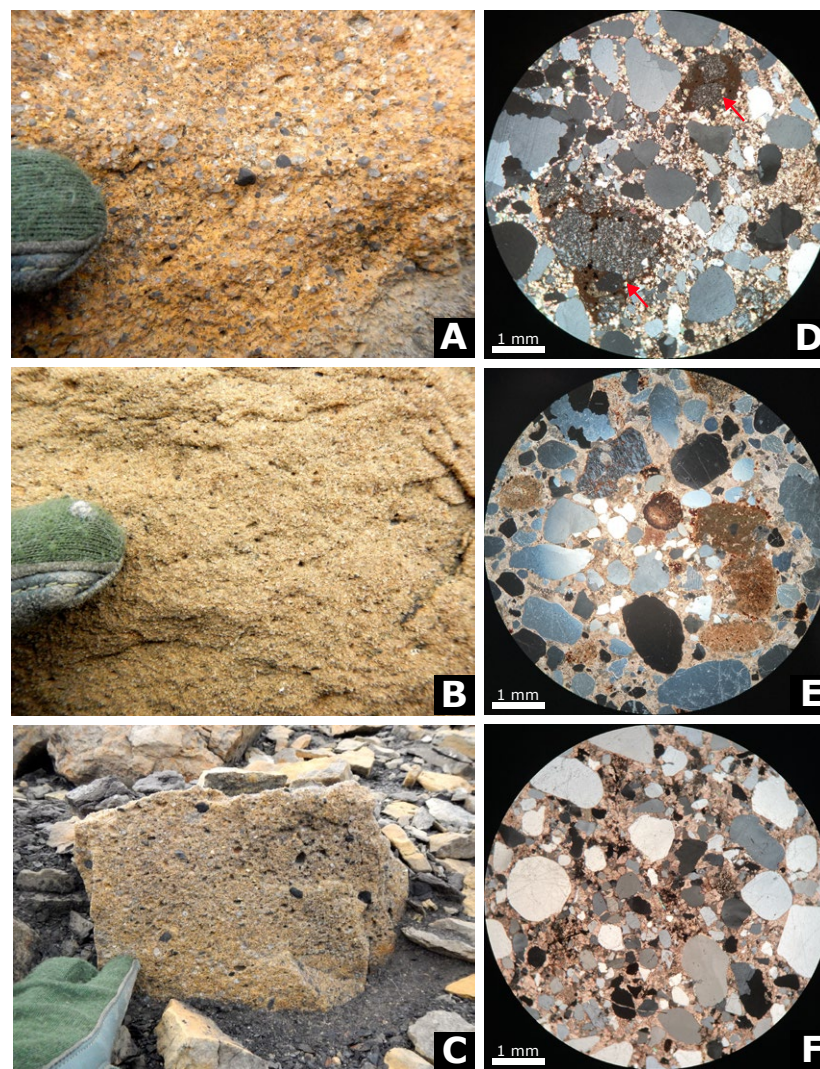
Figure 8. Mesoscopic and microscopic appearance of the injectite material making up the injectite structures of the lower complex. (A) Coarse pebbly sandstone comprising the core of the isolated mounded body mapped in Figure 7 (see text for discussion). (B) Coarse sandstone with millimeter-sized shale fragments observed within a sill structure ~50 m to the NW of the coarse-grained mound described in A. (C) Coarse sandstone with centimeter-sized rounded pebbles in a dike associated with a silty mound ~100 m to the NW of the coarse-grained mound described in A. (D) Rounded and spherical, polycrystalline and monocrystalline quartz grains in ferroan-calcite and sideritic cement; two angular fragments of phosphatic/sideritic and dolomite breccia are present (isolated coarse mounded body; sample M13). (E) Corroded, rounded and spherical quartz grains, with phosphate nodules in ferroan-calcite and sideritic cement (irregular dike protruding from coarse sandstone dome body; sample I5S1). (F) Rounded and spherical quartz grains in ferroan-calcite and sideritic cement (pipe/dike structure located a few meters below the coarse mounded body of A; sample I6S1).

minerals were alkali feldspars (orthoclase, albite, sanidine), plagioclase, siderite, aluminosilicates, chalcopyrite, rutile, white mica, charcoal, and zircon. Carbonaceous material appears as flakes (see Fig. 5E), sometimes including grains from the injectite interior. Apart from monomineralic grains, aggregates (a mixture of aluminosilicates and small grains [<0.1 mm], primarily quartz) were observed as well. Localized cataclastic deformation bands and open fractures were also observed, mainly oriented perpendicular to the injectite's margin (see Fig. 5F).

The injectite material of the lower complex includes unsorted, subrounded to well-rounded grains (between 0.1 mm and 4 cm) embedded in a pale yellow–colored cement. Both roundness and sphericity of the grains vary between 0.5 and 0.9, with an average of 0.7 (see Fig. 11A). Quartz dominates the grain composition (~60%), mainly appearing as monocrystalline quartz, but polycrystalline quartz, chert, and chalcedony were observed as well. Roughly 50% of the quartz grains showed undulose extinction. Other minerals included plagioclase, alkali feldspar (orthoclase, albite, sanidine), glauconite, white mica, biotite, siderite, rutile, pyrite, zircon, aluminosilicates, barite, and carbonaceous flakes (see Fig. 10).

Pyrite appear as subhedral to euhedral crystals and as framboidal pyrite. The framboidal pyrite is mainly accompanied by carbonaceous material. Rutile was observed to overprint organic structures. Also here, aggregates (a mixture of aluminosilicates, calcite, and small grains [<0.1 mm], primarily quartz) were observed.

The cement is composed of ankerite-sparite (Fig. 11B), with pores filled by sheet aluminosilicates (Fig. 11C). Locally, the color of the cement can veer to brownish, being enriched in S and Ti. Some grains show a rim of isopachous ankerite cement, sometimes layered by different color shades. Moreover, microscopic data from the lower complex showed that the percentage of grains with respect to cement increases toward the east.

Most thin sections showed alignment of the grains along the margins of the injectites. Several dikes crosscutting well-lithified silty mounds (Fig. 12A) also showed a systematic zoning, due
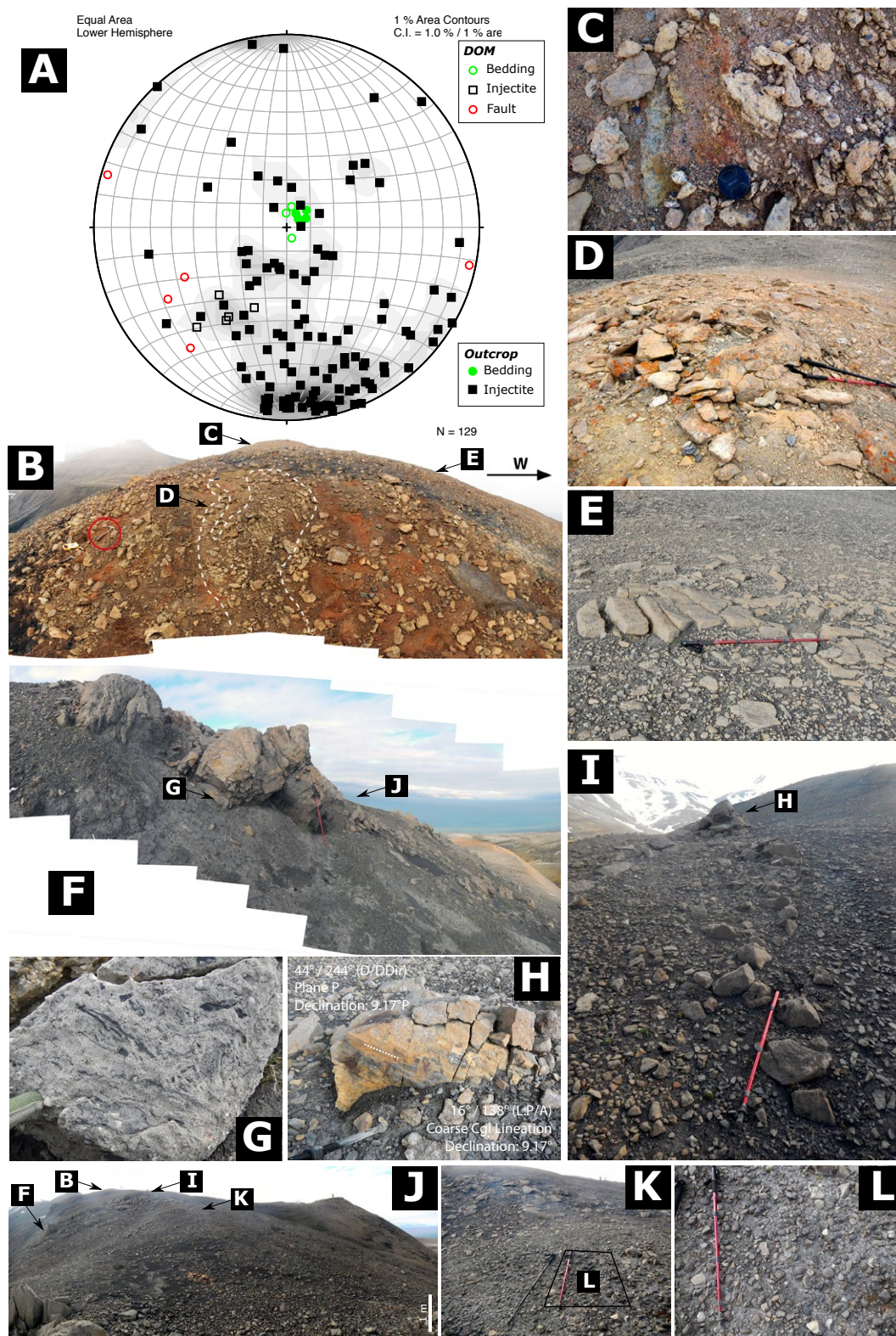
Figure 9. Outcrop appearance and spatial distribution of the injectite structures forming the lower complex. (A) Stereoplot of structural-stratigraphic data from field work and digital outcrop model (DOM) analysis summarizing the injectite structures comprising the lower complex. (B) Vertical and branching pipe-like structure observed a few meters below the isolated mound illustrated in D. Hammer for scale (red circle). Note the strikingly red alteration color of the shales surrounding the structure. (C) Detail of B showing the pebbly sandstone-conglomerate comprising the injection pipe at its margin. (D) Coarse-grained, circular core of the mounded sandstone structure. (E) Systematically fractured pebbly sandstone sill with inverse grading. (F) Photomosaic illustrating the coarse-grained sandstone sill-dike complex surrounding dome structures. (G) Detail of F showing the great amount of disaggregated organic shale material in the sandstones comprising the complex. (H) Linear corrugations and striations gently inclined with respect to bedding on the side of the dike depicted in I. (I) Coarse-grained dike offshooting from the sandstone complex illustrated in F. (J) Isolated conglomeratic dome structure. Walking stick for scale: 1.3 m. (K) Detail of J showing the upper contact of the conglomeratic dome with the surrounding shales through the occurrence of a thin sandstone interval with the same characteristics of F. (L) Detail of K showing the appearance of the poorly consolidated paraconglomerate with rounded clasts comprising the dome structure in J. D/DDir—dip/dip direction; Cgl—conglomerate. L:P/A—lineation:plunge/azimuth.

Ogata et al. | Sediment intrusions in the Agardhfjellet Formation (Svalbard)
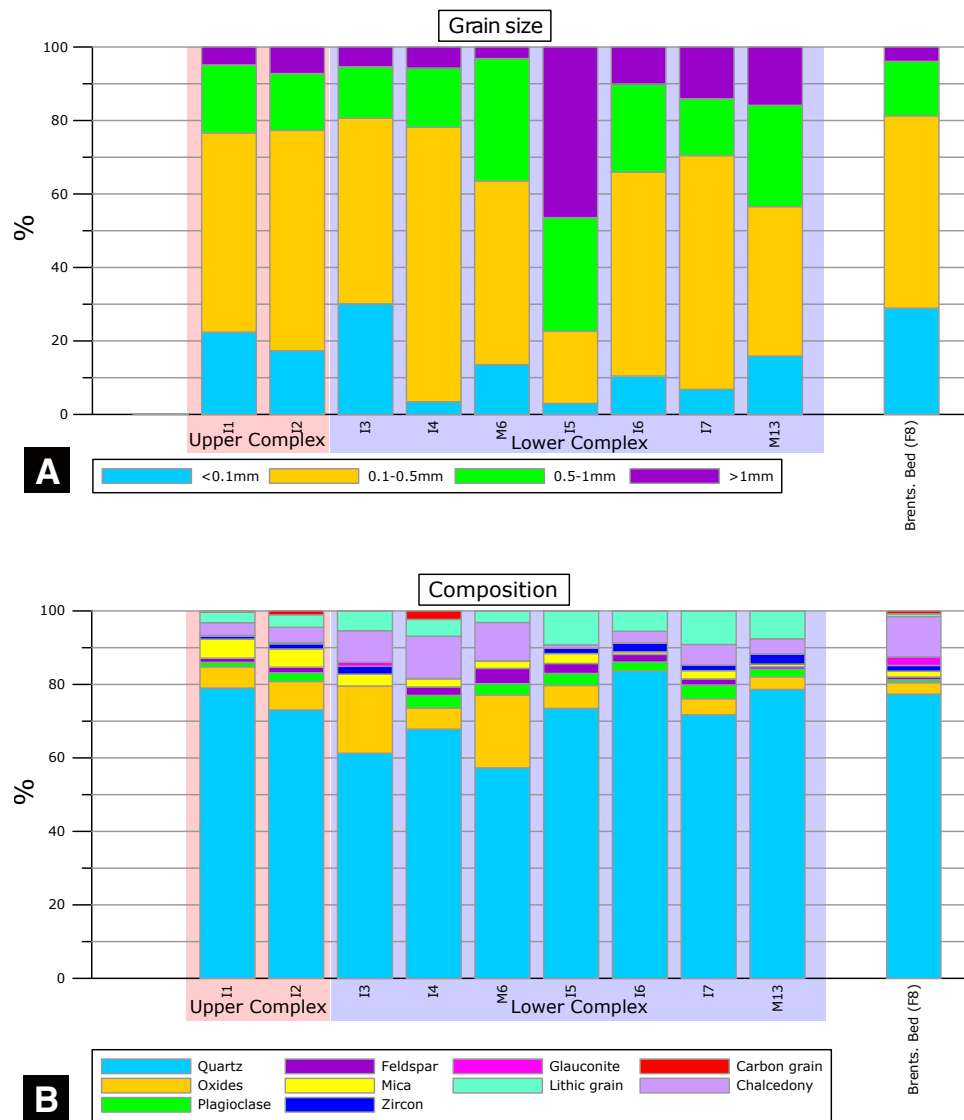
Figure 10. (A) Grain-size distribution and (B) mineral content of upper complex and lower complex samples and comparison with the reference Brentskardhaugen (Brents.) Bed of the Wilhelmøya Subgroup.

to the clear distinction between host rock (zone 1), injectite margin (zone 2), and interior (zone 3), identifiable either at mesoscale (Fig. 12B) or in thin section (Fig. 12C). Analysis of grain types and maximum particle-size distributions within the three architectural elements of these dikes suggested that lithic clasts are concentrated in the core part of the dikes (zone 3), whereas enhanced cementation was observed in both the marginal (zone 2) and core parts (zone 3). Moreover, apart from oxides and organic matter, a gradual systematic increase was observed in grain (clast) size from margins to core (Figs. 12D–12G).

In these dikes, the margin contains a lower percentage of grains than the injectite interior, sometimes bearing outsized clasts up to a few centimeters in size (Figs. 13A–13C). Roughly 60% of these grains are microfractured. Small hairline veins (<0.1 mm), mainly oriented at an angle to the margin of the injectites, are filled by secondary calcite. Bigger open fractures (>0.1 mm) are filled by cement. The larger microfractures are filled with cement and/or secondary calcite and are oriented parallel to the margin of the injectites. Some of these fractures also crosscut the cement and other grains (Figs. 13D–13F).

■ DISCUSSION

Based on the results presented here, we discuss the two investigated sedimentary injection complexes in terms of possible source(s) of the injected material and subsurface remobilization and flow processes, with considerations on the environmental conditions of formation.

Possible Source(s) and Provenance

Compositionally, both the upper complex and lower complex show similar characteristics. In particular, they contain different types of quartz grains: monocrystalline, polycrystalline with undulose extinction, chert, and chalcedony. These grains are expected to form in different geologic settings, suggesting different amounts of sedimentary
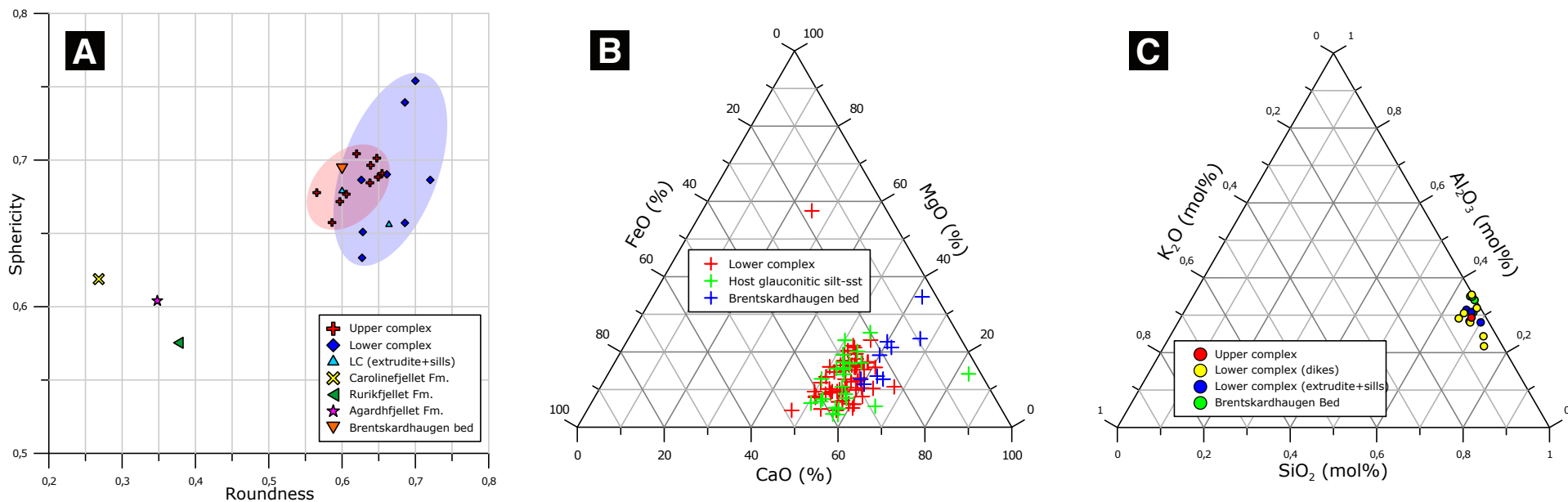
Figure 11. (A) Sphericity vs. roundness, (B) clay matrix mineralogy, and (C) cement composition plots of upper complex, lower complex (LC), and surrounding reference lithologies. Note that no appreciable amount of cement was available for upper complex. Sst—sandstone.

transport before remobilization and injection. The high content of such grains (~60%) points toward a silica-enriched source, also characterized by the occurrence of both marine fossils and wood fragments (up to tens of centimeters in size). Moreover, detrital grains show systematically corroded rims and weathered parts, along with differential cementation and a heterogeneous matrix, testifying for enhanced diagenetic conditions.

Black shale clasts most likely originated from the Agardhfjellet Formation, as they only appear on the margins of the injectites, due to abrasion of the host rock during the injection process (Cobain et al., 2015).

From a micromorphological point of view, both the upper complex and lower complex show comparable values of sphericity and roundness of the constituent grains, with strikingly high values compared to the surrounding and overlying lithologies.

A good match is instead observed with the characteristics of the underlying Wilhelmøya Subgroup and specifically with the Brentskardhaugen Bed (Fig. 14A). Moreover, diagnostic detrital Cr-spinel typically found in the De Geerdalen Formation (Mørk, 2013) has been documented in the lower complex (SEM point measurement B1; sample I6S1–2), possibly indicating an even deeper contribution from the underburden.

Injection Process, Paleo–Fluid Flow, and Diagenesis

The structures and internal fabric observed within the upper complex such as the ridged bounding surfaces, the vertical-lateral tapering, the massive appearance, and the internal zoning point toward a laminar flow type as the dominant

injection process, occurring at relatively high confining pressure (Taylor, 1982; Cobain et al., 2015).

Notably, little cement is present in the upper complex, with the stratigraphically lower parts being completely unconsolidated and implying a buffering fluid, keeping together the grains during injection. Given the occurrence of bituminous fragments and the organic-rich host formation, an influx of hydrocarbons, both as oil and gas, is indicated. In the lower complex, both the internal features and the overall architecture—such as the irregular contacts with the host rock; clay smear on the margins; internal grading and zoning; shape, size, and position of the rip-up mudstone clasts; and the generalized soft-sediment deformation—suggest mixed flow conditions, likely laminar at first and then turbulent achieved at low confining pressure (Peterson, 1968; Kawakami and Kawamura, 2002; Huuse et al., 2005; Hubbard et al., 2007; Ross et al.,
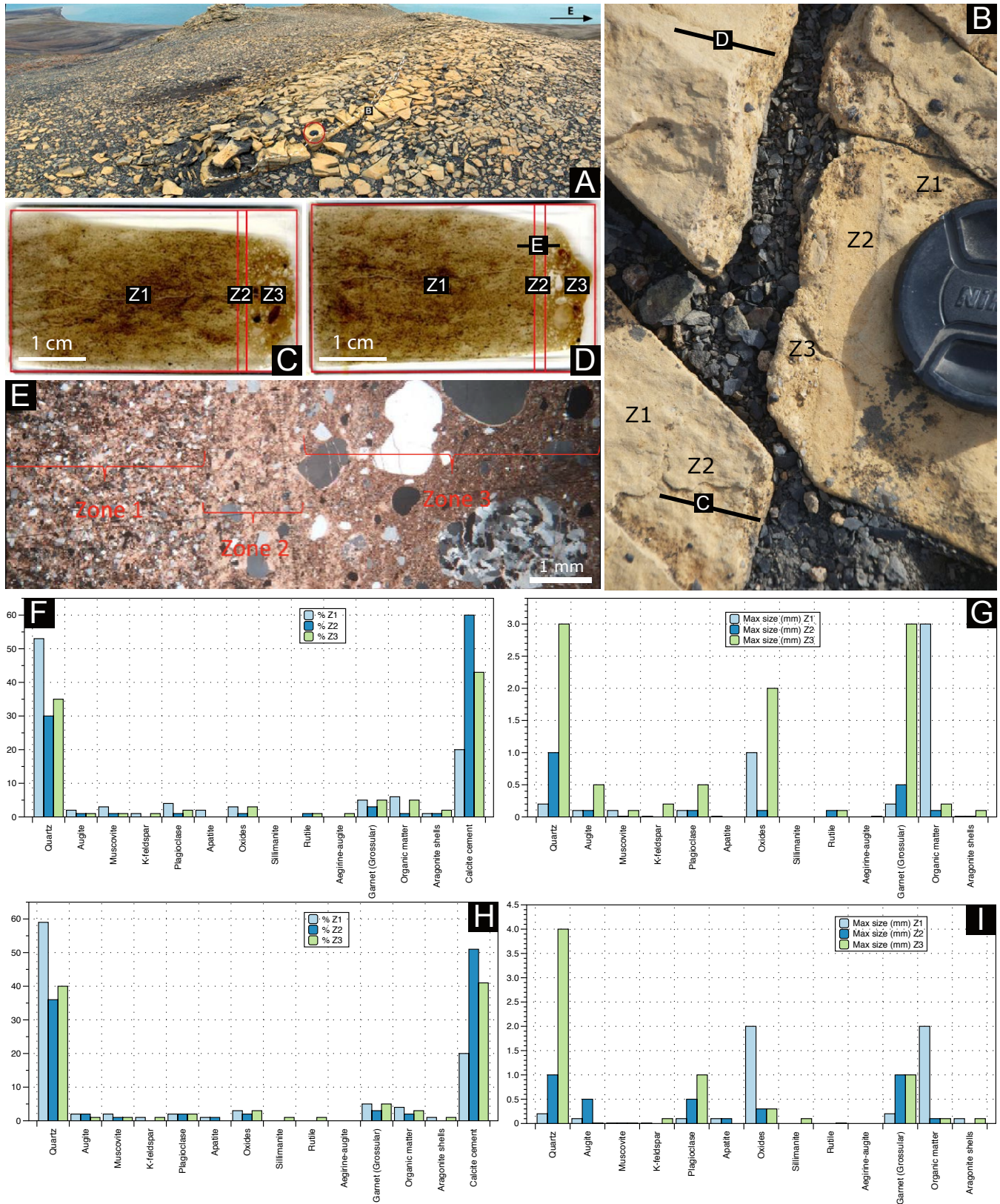
Figure 12. Outcrop to microscopic appearance of centimeter-thick dikes of the lower complex associated with silty mounds. (A) Well-consolidated silty mound intervals crosscut by a centimeter-thick, coarse-grained dike (white dashed line). (B) Detail of A showing the internal architecture of the dike, subdivided in zones 1 (pristine host rock), 2 (margin/transition), and 3 (core; see text for discussion), and locations of analyzed thin sections. (C–D) Representative thin sections; location shown in B. (E) Dike architecture and zoning in thin section (location in D). (F) Relative abundance (percentage) of clasts in thin section C subdivided according to mineralogy and location within the injectite anatomy. (G) Maximum grain size (mm) of clasts in thin section C subdivided according to mineralogy and location within the injectite anatomy. (H) Relative abundance (percentage) of clasts in thin section D subdivided according to mineralogy and location within the injectite anatomy. (I) Maximum grain size (mm) of clasts in thin section D subdivided according to mineralogy and location within the injectite anatomy.
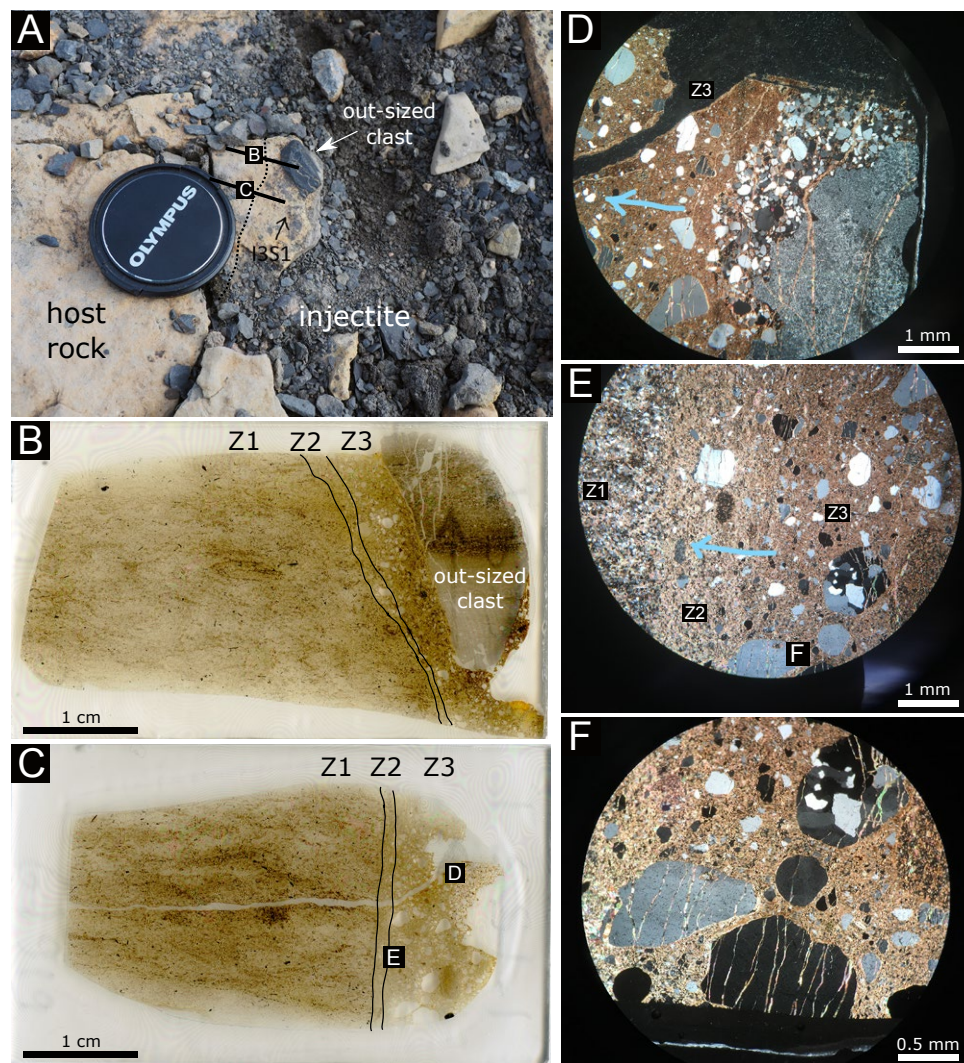
Figure 13. Mesoscopic to microscopic anatomy of centimeter-thick dikes of the lower complex associated with silty mounds (sample I3S1). (A) Dike bearing a centimeter-sized, subrounded dolomite clast; sampling point and locations of thin sections are labeled. (B–C) Representative thin sections with internal zoning labeled; location shown in A. (D) Clustering of grains in the pressure-shadow zones of millimeter-sized clast; light blue arrow indicates the direction of the dike margin (location in C). (E) Detail of texture and fabric of the internal zoning; light blue arrow indicates the direction of the dike margin (location in C). (F) Detail of E highlighting the dike-parallel hairline calcite veins and rims, which are in optical continuity with the cement.

2011, 2014; Quigley et al., 2013; Scott et al., 2013; Cobain et al., 2015). Such conditions fit with a shallow "plumbing" system that was subsequently connected with a paleo-seafloor (i.e., glauconite-rich, hardground-type interval; Boehm and Moore, 2002; Cobain et al., 2015).

This scenario is supported by mineralogical features. In this framework, soon after emplacement, rims around the grains formed as a result of weak reducing conditions in the formation water, and the exchange between pore water and seawater. Later, more fresh seawater was available to form sparite. Afterward, pores within the sparite were filled by aluminous clays.

The large occurrence of framboidal pyrite suggests microbial activity within the injectites after emplacement (Krumholz et al., 1997; Machel and Foght, 2000; Parkes et al., 2005; Fredrickson and Balkwill, 2006; Parnell et al., 2013), as also suggested by the occurrence of barite crystals (e.g., Hanor, 2000). Their association with pyrite crystals may testify to local microbial enrichment of barium in a sulfate-rich environment (Martínez-Ruiz et al., 2019).

Another notable difference between the lower complex and upper complex is in the amount and location of glauconite, which is mostly concentrated at the injectite margins in the upper complex. This may suggest that differential weathering, and therefore a younger age for the upper complex, provided less time to alter the injectite from the interior to the margins, or segregation by velocity gradients in the laminar flow (Fig. 14B).

Localized intragranular fractures filled by matrix material were systematically observed in both the upper complex and lower complex, whereas a diffuse crosscutting intergranular, anastomosing calcite vein set oriented parallel to the injection margin was observed in the lower complex. In terms of deformation mechanisms, the former are interpreted to record particulate flow with localized grain breakage in fluid-overpressure conditions, whereas the latter may indicate the subsequent hydrofracturing of the packed granular network. In the latter scenario, the hydrofracturing event could have been related to the renewed pulse of fluid overpressure responsible for the formation of the upper complex, along with its connection with the lower complex.
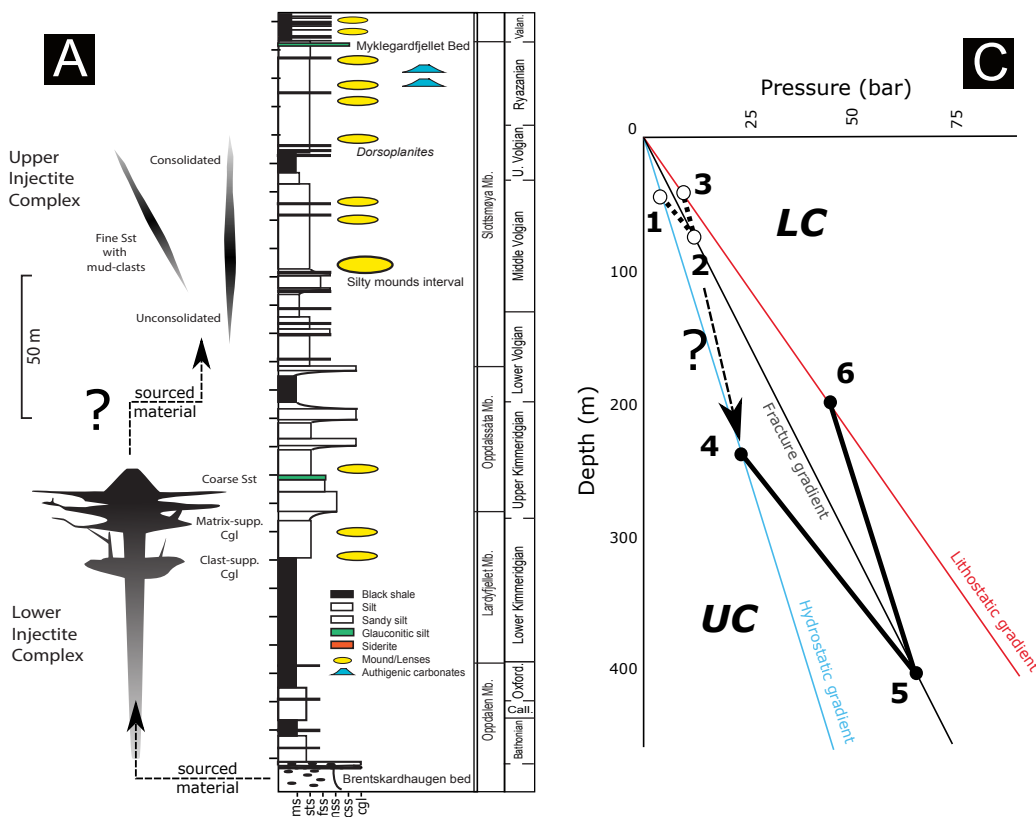
Figure 14. (A) Synoptic stratigraphic chart showing the stratigraphic position and inferred relationships between the upper complex and lower complex. (B) Conceptual cartoon showing development of the injection process for the lower complex (LC) (1, 2, 3) and upper complex (UC) (4, 5, 6). The yellow material represents the parent unit and injected material. 1—Pre-injection and trigger, where overpressure is due to interplay between near-surface loading fluctuations and localized diagenetic fronts related to hardground (condensed) intervals. 2—Migration, with lateral and vertical pressure transfer before connecting to the surface (laminar flow regime). 3—Emplacement, after connection with the surface (turbulent flow regime). 4—Pre-injection and trigger, as for 1, but at the expenses of already injected (and extruded) clastic material. 5—Migration, with vertical pressure transfer and propagation with laminar flow. 6—Emplacement, with lateral (along-strike) pressure transfer and propagation with laminar flow. (C) Qualitative diagram illustrating the inferred pressure-depth paths for the UC and LC as depicted in B. Gradients are from Longyearbyen CO$_2$ Laboratory. Sst—sandstone; Cgl—conglomerate; Call.—Callovian; Valan—Valanginian. ms—mudstone; sts—siltstone; fss—fine sandstone; mss—medium sandstone; css—coarse sandstone.

Linear features such as corrugations, mullion-like structures, and soft-sediment striations were observed in both the upper complex and lower complex dikes, showing a gentle angle with respect to the overall bedding (up to 40°). These structures suggest at least a partially oblique flow of material through the dikes. Along with these characteristics of the contact surfaces, the transition from injectite material to the host rock is different for the upper complex and lower complex. In the former, this transition is sharp, even where there is no competence contrast due to unconsolidated material, suggesting injection of remobilized material into competent lithologies by cracking and filling. On the other hand, in the lower complex, both sills and dikes show an internal architecture that defines a gradual transition from the injected material to the country lithology at the microscale, with the occurrence of a transitional zone of mixing (zone 2) separating the core of the structure from the host rock, which indicates relatively low competence contrast during emplacement (i.e., injection into partly lithified sediments).

Emplacement Conditions, Timing, and Diagenesis

The lower complex is interpreted as a shallow injectite system, developed by remobilization of clastic material up to a few tens of meters deep into the subsurface, with associated extrusion to the surface (Figs. 14B and 14C). The evidence for mixed laminar and turbulent flow (e.g., grading, erosive margins, flow structures) and the abundance of concordant intrusions that are gently inclined with respect to bedding (sills vs. dikes) support such shallow burial conditions. Such a framework constrains the timing of emplacement to the age of the paleo-seafloor (i.e., glauconite-rich hardground interval) onto which the "extrusive body" (i.e., sand volcano) was built. This interval is located at the boundary between the Late Jurassic Lardyfjellet and Oppdalssåta Members, marking the transition between the Lower and Upper Kimmeridgian.

Due the locally poor outcrop conditions (i.e., fracturing and frost heave in the permafrost process zone), and given the sedimentological features of the stratigraphically concordant thin sills identified around the mounded pebbly sandstone body in the lower complex (i.e., inverse grading, sharp top and bases, and grain-size reduction from the injectite complex), an alternative origin as local grain flows sourced from the mounded structure (i.e., sand volcano) can be also outlined. In this framework, these layers would record phases of enhanced sand extrusions at the seafloor during the construction of the mounded structure.

Moreover, around the same stratigraphic level of the lower complex (i.e., condensed sections/hardgrounds), isolated silty mounds/lenses were often observed to contain scattered rounded pebbles up to centimeters in size (along with plant fragments and other organic material), which were remarkably similar to the ones reported in the injectite material, suggesting the possibility of formation as minor, finer-grained extrusive bodies (i.e., mud volcanoes).

In contrast, features of the upper complex indicate formation at a relatively deeper stratigraphic level, in the order of hundreds of meters (see Figs. 14B and 14C). The systematic occurrence of features related to laminar flow and the preferred vertical orientation at high angle with respect the bedding support the interpretation of higher confining pressure due to deeper burial. Here, the timing of emplacement can be indirectly constrained on the basis of the crosscutting relationships with tectonic features. The sedimentary dikes of the upper complex appear to be segmented and displaced by low-angle and layer-parallel shears attributed to the development of the West Spitsbergen fold-and-thrust belt. In this framework, the upper complex therefore predates the Paleogene and was likely emplaced roughly within the Cretaceous.

The injectites comprising the upper complex are poorly consolidated in the (stratigraphically) lower part. This underconsolidation is possibly due to hydrocarbon charging leading to quartz/calcite cement inhibition, as suggested by this vertical zoning, the higher organic content of surrounding shales, and the occurrence of bituminous remnants in the injected material. On the other hand, injectites making up the lower complex are well consolidated due to a widespread, multigeneration ferroan-calcite and ankerite cementation (see Supplemental Material).

Possible Preconditioning Factors and Triggers

Possible triggering mechanisms for the injectite complexes can be identified within the context of existing literature, likely being of tectonic and/or climatic origin. Specifically, the shallow lower complex appears to be related to a transgressive phase following a period of high-frequency sea-level fluctuations responsible for the development of the regional condensed sections of the Wilhelmøya Subgroup and the laterally extensive hardgrounds of the lower Agardhfjellet Formation (Koevoets et al., 2019). In this framework, rapid sea-level changes may have caused fluid pressure buildup below the well-cemented (less permeable) condensed sections/hardgrounds (Sultan et al., 2020), leading to shallow subsurface sediment remobilization, intrusion, and extrusion at the seafloor (see Fig. 14B). The presence of Triassic faults in the underburden (Mulrooney et al., 2019) might have played a role in triggering and localizing the intrusions, by influencing the pathways of subsurface fluid circulation and providing sites for reactivation via seismic shocks or shear-induced liquidization, leading to fluid pressure release.

Deeper crustal processes are suggested for the injectites of the upper complex, along with a stronger structural control. The two main directions recorded by the two dikes of the upper complex (N50° and N85°) are coherent with the local stress field rotation during the tectonic evolution of Svalbard through the Cenozoic (e.g., Ogata et al., 2014; Maher et al., 2020). Such conditions, and the documented occurrence of similar dikes elsewhere in Svalbard within the same stratigraphic interval (Senger et al., 2014; Maher et al., 2020), suggest regional endogenic processes such as earthquakes as possible triggers for sediment remobilization. Local enhanced siderite cementation in this siltier interval may have provided the necessary permeability barrier for the (over)pressure buildup (see Fig. 14B). Another possible trigger for injection is

the almost coeval Mjølnir impact event, dated at 145 Ma (Tsikalas et al., 2010). The cogenetic Sindre ejecta bed has been traced in the study area (Dypvik et al., 1991), ~40 m above the stratigraphic level into which the upper complex dikes die out (i.e., close to the Myklegardfjellet bed; see Figs. 2 and 14A).

As a final note, our data suggest at least a partly common source of the remobilized material for both the lower complex and upper complex (see Data and Results section above), outlining a scenario of long-term connection between the two complexes. In this framework, the lower complex material would have been remobilized again after its burial and reworked/recycled into the upper complex injectites as testified by morphometrical analyses (see Fig. 11A).

Conceivably, the emplacement precursors of the High Arctic large igneous province (HALIP) dolerite complexes played a role (Senger et al., 2014). In this framework, the textural differences observed for the lower complex and upper complex (resulting in fully cemented with low matrix and partly unconsolidated with high matrix structures, respectively) could be explained by an elutriation process related to the forced flow of hydrothermal fluids (e.g., Ross and White, 2005). The occurrence of quartz and feldspar overgrowth on corroded boundaries marked by dust rims and illitization of feldspars (see Supplemental File S2a; Figs. S5A and S29) qualitatively supports this interpretation (Haile et al., 2019). Moreover, because the connection of the upper complex with hydrocarbon seeps on Janusfjellet, as suggested by Hammer et al. (2011), seems to be supported by our results (see Data and Results section above), a combination of these two processes could be outlined (i.e., hydrothermally induced overmaturation of source rock; Senger et al., 2017). Further specific petrographic-geochemical analyses (e.g., SEM, cathodoluminescence [CL], X-ray fluorescence [XRF]) are envisioned to verify and confirm such relationships.

Implications for Top-Seal Integrity and Fluid Circulation

Sandstone injectites represent significant structural heterogeneities (e.g., Hurst et al., 2011; Templeton et al., 2006), with typically high porosity and permeability, up to 40% and 7 D (darcies), respectively (Pernin et al., 2022). In some cases, such as UK Corona discovery well 9/a7a-39a,39z, enough sand was remobilized to form complex interconnected injectite reservoirs that reach several hundred meters above the parent body and host commercial quantities of producible hydrocarbons (Pernin et al., 2022).

Given their complex geometries, injectites can also represent drilling hazards or a risk for locally compromising the top-seal integrity, especially if drilling passes through the permeable injectite unit. This is especially true when the sand was, as we envision for this case study, emplaced from the underlying reservoir interval.

The Wilhelmøya Subgroup is the main reservoir targeted for potential CO_2 storage beneath Longyearbyen (Rismyhr et al., 2019; Mulrooney et al., 2019). The time-equivalent unit, the Realgrunnen Subgroup (Lord et al., 2019), is the major reservoir for producing hydrocarbon fields (i.e., Snøhvit, Goliat, Johan Castberg), discoveries (i.e., Wisting), and offshore CO_2 storage sites (i.e., Snøhvit). In Svalbard, the sequence offers a matrix permeability of up to 2 mD and matrix porosity of up to 20% (Senger et al., 2015). While the lower injection complex reaches 49 m above its base, the upper injection complex breaches the overlying lower cap rock (Agardhfjellet Formation) by 150 m.

The Agardhfjellet Formation is affected by numerous structural heterogeneities across the reservoir-seal interface, including the presented sandstone injectites, fault zones (Lubrano-Lavadera et al., 2019), and an igneous dike. All of these represent potential CO_2 leakage pathways, and a critical understanding of the injectite geometry and its fluid-flow properties compared to the host rock is crucial to limiting the risk both in Svalbard and elsewhere.

Injectites would pose not just a risk to the cap rock in terms of a permeability pathway, but they can also accommodate larger hydrocarbon columns above the reservoir, resulting in buoyancy overpressure. This means the crest of the hydrocarbon column is shallower, resulting in a lower fracture pressure at that point in the encompassing shale seal. This is something that needs to be considered for CO_2 injection; while buoyancy is less likely to be problematic, the lower-than-expected fracture gradient (or shallower crest) may be critical if injectites overlie the reservoir at the injection site.

While overpressure must have been present to form the injectites in the geological past, at the Longyearbyen CO_2 Laboratory, the Wilhelmøya Subgroup is strongly underpressured (65 bar below sea-level hydrostatic pressure). It is considered that the underpressure originated due to deglaciation over the past tens of thousands of years, resulting in decompaction of the overlying shales, which transferred to the reservoir (Birchall et al., 2020).

Other evidence of fluid flowing from the reservoir into the cap rock exists in strontium isotope data, which indicate fluid has entered the cap rock from below at some point in the recent geological past (Huq et al., 2017). It is possible that injectites locally enhance connectivity with the shale to aid their equilibration, though it should be noted that the low permeability of the reservoir has helped to prevent underpressure dissipating laterally to outcrops 15 km from the CO_2 laboratory.

Notably, the cap-rock interval onshore Svalbard is an excellent direct analogue for the regional cap rocks of the Hekkingen and Fuglen Formations (Paulsen et al., 2022) in the southwestern Barents Sea, where sandstone injectites have been encountered in at least two exploration boreholes. Detailed field studies as presented herein provide robust data that will ideally be used as input to future fluid-flow simulations to reduce drilling risk and ascertain the possible upside potential to the underlying hydrocarbon-bearing intervals.

■ CONCLUSIONS

Sedimentary injectites can be found in many geological settings, and they have a recognized importance in subsurface exploration and exploitation (e.g., Jolly and Lonergan, 2002; Hurst et al., 2011; Cobain et al., 2015, 2017). Knowledge mainly derives from geophysical surveys, but outcrop-scale observations are needed to fully unravel finer details, especially in terms of formation, fluid circulation, and diagenetic processes.

The mesoscale sedimentary injections occurring in the Middle Jurassic–Lower Cretaceous

Agardhfjellet Formation in Svalbard (Arctic Norway) allow high-resolution structural-stratigraphic investigations within a continuously exposed and geologically well-constrained framework. Two sedimentary injection complexes showing different emplacement mechanisms and boundary conditions were investigated in this study at different stratigraphic levels. The upper complex comprises two narrow and roughly tabular clastic dikes, tens of centimeters wide and laterally and vertically traceable for tens of meters, composed of an unsorted, muddy, fine- to medium-grained sandstone with angular silty shale and lithic clasts. These dikes show two main orientations, striking NE-SW (N50°) and E-W (N85°), with the former dike showing a sharp kink in the upper part (toward the S), where it becomes subparallel to the direction of the E-W dike, wedging out near the contact with the overlying Rurikfjellet Formation.

Soft-sediment corrugation was observed in the outer walls of these dikes, highlighting a systematic lineation pattern subparallel to the bedding, likely suggesting lateral-oblique emplacement of the infilling material rather than the expected vertical emplacement. Another peculiar feature of this upper injectite system relates to lithification; in fact, the injectites are thickest and most consolidated in the upper–middle parts of the exposure, whereas they become poorly to unconsolidated downward, requiring excavation to trace them. Such "inverse" differential consolidation is possibly due to the higher organic content of the country rock, possibly leading to inhibition of cementation. Finally, these injectites appear to be segmented, being crosscut and displaced by subhorizontal, striated shear surfaces with lateral movement up to 1 m, likely due to Cenozoic compression related to the development and evolution of the West Spitsbergen fold-and-thrust belt.

The stratigraphically lower sedimentary injection complex consists of a network of thin clastic dikes and sills developed as tens-of-meters–sized, pipe-like structures consisting of clast- to matrix-supported, fine- to medium-grained, pebbly sandstones and conglomerates. The centimeters-thick, subvertical dikes are subdivided into three main sets oriented NE-SW (N34°), NNW-SSE (N154°), and ENE-WSW

(N80°), which appear to be connected by sills. Subhorizontal lineations similar to those described for the upper complex were also observed at dike margins. Both the thickness and grain size of dikes and sills seem to increase toward the E, where isolated bodies of conglomerates appear to be distributed at different stratigraphic levels, across an interval of ~80 m, and characterized by complex internal features (e.g., folding) and boundaries. The coarser clastic elements and the appearance of the matrix seem to belong to the lithologies comprising the immediately underlying Wilhelmøya Subgroup. Both the upper and lower injectite complexes are related to structural lineaments oriented WNW-ESE and NNE-SSW, respectively. In particular, these directions are parallel to the regional tectonic trend defined by the structures of the West Spitsbergen fold-and-thrust belt and the orientation of the Lomfjorden and Billefjorden fault zones (see Figs. 1B and 1C), suggesting some structural control on their development.

Isolated mounds of diagenetic origin are interpreted as having developed at the paleo-seafloor in connection with condensed sections/hardgrounds, as indicated by glauconite-rich and fossiliferous intervals. The relationships indicate a strong interplay among surficial processes, fluid circulation, and the subsurface structural network. Such subsurface remobilization and consequent intrusion (and extrusion) were achieved by the lower complex during the Late Jurassic at relatively shallow burial conditions (tens of meters), whereas the upper complex developed at higher confinement pressure (hundreds of meters of burial), most likely during the Late Cretaceous.

This study illustrates the crucial importance of field-based data to constrain the long-lived spatiotemporal relationships among sedimentary intrusions and synemplacement and postemplacement processes and obtain a broader understanding of these units, which leads to correct upscaling to observations made at the seismic scale in many modern subsurface scenarios.

REFERENCES CITED

Bergh, S.G., Braathen, A., and Andresen, A., 1997, Interaction of basement-involved and thin-skinned tectonism in the Tertiary fold-thrust belt of central Spitsbergen, Svalbard: American Association of Petroleum Geologists Bulletin, v. 81, no. 4, p. 637–661, https://doi.org/10.1306/522B43F7 -1727-11D7-8645000102C1865D.

Birchall, T., Senger, K., Hornum, M.T., Olaussen, S., and Braathen, A., 2020, Underpressure in the northern Barents shelf: Causes and implications for hydrocarbon exploration: American Association of Petroleum Geologists Bulletin, v. 104, no. 11, p. 2267–2295, https://doi.org/10.1306/02272019146.

Boehm, A., and Moore, J.C., 2002, Fluidized sandstone intrusions as an indicator of paleostress orientation, Santa Cruz, California: Geofluids, v. 2, no. 2, p. 147–161, https://doi.org /10.1046/j.1468-8123.2002.00026.x.

Braathen, A., Bergh, S.G., and Maher, H.D., Jr., 1995, Structural outline of a Tertiary basement-cored uplift/inversion structure in western Spitsbergen, Svalbard: Kinematics and controlling factors: Tectonics, v. 14, no. 1, p. 95–119, https:// doi.org/10.1029/94TC01677.

Braathen, A., et al., 2012, The Longyearbyen CO$_2$ Lab of Svalbard, Norway—Initial assessment of the geological conditions for CO$_2$ sequestration: Norwegian Journal of Geology, v. 92, no. 4, p. 353–376.

Bradaric, A.D., Andersen, T., Lecomte, I., Løseth, H., and Eide, C.H., 2022, Recognition and characterization of small-scale sand injectites in seismic data: Implications for reservoir development: Journal of the Geological Society, v. 179, no. 2, https://doi.org/10.1144/jgs2021-041.

Cobain, S.L., 2016, Mechanisms, Distribution, and Subsurface Implications of Clastic Injectites [Ph.D. dissertation]: Leeds, UK, University of Leeds, 208 p.

Cobain, S.L., Peakall, J., and Hodgson, D.M., 2015, Indicators of propagation direction and relative depth in clastic injectites: Implications for laminar versus turbulent flow processes: Geological Society of America Bulletin, v. 127, no. 11–12, p. 1816–1830, https://doi.org/10.1130/B31209.1.

Cobain, S.L., Hogson, D.M., Peakall, J., and Shiers, M.N., 2017, An integrated model of clastic injectites and basin floor lobe complexes: Implications for stratigraphic trap plays: Basin Research, v. 29, no. 6, p. 816–835, https://doi.org/10 .1111/bre.12229.

Collignon, M., and Hammer, Ø., 2012, Petrography and sedimentology of the Slottsmøya Member at Janusfjellet, central Spitsbergen: Norwegian Journal of Geology, v. 92, p. 89–101.

Dallmann, W.K., ed., 2015, Geoscience Atlas of Svalbard: Tromsø, Norway, Norsk Polarinstitutt, 292 p.

Dypvik, H., Eikeland, T.A., Backer-Owe, K., Andresen, A., Johanen, H., Elverhøi, A., Nagy, J., Haremo, P., and Biærke,

T., 1991, The Janusfjellet Subgroup (Bathonian to Hauterivian) on central Spitsbergen: A revised lithostratigraphy: Polar Research, v. 9, no. 1, p. 21–44, https://doi.org/10.3402/polar.v9i1.6777.

Eldholm, O., Faleide, J.I., and Myhre, A.M., 1987, Continent-ocean transition at the western Barents Sea/Svalbard continental margin: Geology, v. 15, no. 12, p. 1118–1122, https://doi.org/10.1130/0091-7613(1987)15<1118:CTATWB>2.0.CO;2.

Faleide, J.I., Tsikalas, F., Breivik, A.J., Mjelde, R., Ritzmann, O., Engen, Ø., Wilson, J., and Eldholm, O., 2008, Structure and evolution of the continental margin off Norway and the Barents Sea: Episodes, v. 31, no. 1, p. 82–91, https://doi.org/10.18814/epiiugs/2008/v31i1/012.

Fredrickson, J.K., and Balkwill, D.L., 2006, Geomicrobial processes and biodiversity in the deep terrestrial subsurface: Geomicrobiology Journal, v. 23, no. 6, p. 345–356, https://doi.org/10.1080/01490450600875571.

Grippa, A., Hurst, A., Palladino, G., Iacopini, D., Lecomte, I., and Huuse, M., 2019, Seismic imaging of complex geometry: Forward modeling of sandstone intrusions: Earth and Planetary Science Letters, v. 513, p. 51–63, https://doi.org/10.1016/j.epsl.2019.02.011.

Haile, B.G., Czarniecka, U., Xi, K., Smyrak-Sikora, A., Jahren, J., Braathen, A., and Hellevang, H., 2019, Hydrothermally induced diagenesis: Evidence from shallow marine–deltaic sediments, Wilhelmøya, Svalbard: Geoscience Frontiers, v. 10, no. 2, p. 629–649, https://doi.org/10.1016/j.gsf.2018.02.015.

Hammer, Ø., and Nakrem, H.A., 2010, Clastic dykes from the Upper Jurassic of Svalbard, Norway: NGF Abstracts and Proceedings, v. 1, no. 1, p. 61.

Hammer, Ø., Nakrem, H.A., Little, C.T.S., Hryniewicz, K., Sandy, M.R., Hurum, J.H., Druckenmiller, P., Knutsen, E.M., and Høyberget, M., 2011, Hydrocarbon seeps from close to the Jurassic-Cretaceous boundary, Svalbard: Palaeogeography, Palaeoclimatology, Palaeoecology, v. 306, no. 1–2, p. 15–26, https://doi.org/10.1016/j.palaeo.2011.03.019.

Hanor, J.S., 2000, Barite-celestine geochemistry and environments of formation: Reviews in Mineralogy and Geochemistry, v. 40, no. 1, p. 193–275, https://doi.org/10.2138/rmg.2000.40.4.

Harland, W.B., 1997a, Central western Spitsbergen, in Harland, W.B., eds., The Geology of Svalbard: Geological Society, London, Memoir 17, p. 154–178, https://doi.org/10.1144/GSL.MEM.1997.017.01.09.

Harland, W.B., 1997b, The Geology of Svalbard: Geological Society, London, Memoir 17, 521 p., https://doi.org/10.1144/GSL.MEM.1997.017.01.26.

Helland-Hansen, W., 2010, Facies and stacking patterns of shelf-deltas within the Palaeogene Battfjellet Formation, Nordenskiöld Land, Svalbard: Implications for subsurface reservoir prediction: Sedimentology, v. 57, no. 1, p. 190–208, https://doi.org/10.1111/j.1365-3091.2009.01102.x.

Hubbard, S.M., Romans, B.W., and Graham, S.A., 2007, An outcrop example of large-scale conglomeratic intrusions sourced from deep-water channel deposits, Cerro Toro Formation, Magallanes basin, southern Chile, in Hurst, A., and Cartwright, J., eds., Sand Injectites: Implications for Hydrocarbon Exploration and Production: American Association of Petroleum Geologists Memoir 87, p. 199–207, https://doi.org/10.1306/1209863M873265.

Huq, F., Smalley, P.C., Mørkved, P.T., Johansen, I., Yarushina, V., and Johansen, H., 2017, The Longyearbyen CO_2 Lab: Fluid communication in reservoir and caprock: International Journal of Greenhouse Gas Control, v. 63, p. 59–76, https://doi.org/10.1016/j.ijggc.2017.05.005.

Hurst, A., Scott, A., and Vigorito, M., 2011, Physical characteristics of sand injectites: Earth-Science Reviews, v. 106, no. 3–4, p. 215–246, https://doi.org/10.1016/j.earscirev.2011.02.004.

Huuse, M., Shoulders, S.J., Netoff, D.I., and Cartwright, J., 2005, Giant sandstone pipes record basin-scale liquefaction of buried dune sands in the Middle Jurassic of SE Utah: Terra Nova, v. 17, no. 1, p. 80–85, https://doi.org/10.1111/j.1365-3121.2004.00587.x.

Jolly, R.J.H., and Lonergan, L., 2002, Mechanisms and controls on the formation of sand intrusion: Journal of the Geological Society, v. 159, p. 605–617, https://doi.org/10.1144/0016-764902-025.

Kawakami, G., and Kawamura, M., 2002, Sediment flow and deformation (SFD) layers: Evidence for intrastratal flow in laminated muddy sediments of the Triassic Osawa Formation, northeast Japan: Journal of Sedimentary Research, v. 72, no. 1, p. 171–181, https://doi.org/10.1306/041601720171.

Koevoets, M.J., Abay, T.B., Hammer, Ø., and Olaussen, S., 2016, High-resolution organic carbon–isotope stratigraphy of the Middle Jurassic–Lower Cretaceous Agardhfjellet Formation of central Spitsbergen, Svalbard: Palaeogeography, Palaeoclimatology, Palaeoecology, v. 449, p. 266–274, https://doi.org/10.1016/j.palaeo.2016.02.029.

Koevoets, M.J., Hammer, Ø., Olaussen, S., Senger, K., and Smelror, M., 2019, Integrating subsurface and outcrop data of the Middle Jurassic to Lower Cretaceous Agardhfjellet Formation in central Spitsbergen: Norwegian Journal of Geology, v. 99, p. 213–246, https://doi.org/10.17850/njg98-4-01.

Krumholz, L.R., McKinley, J.P., Ulrich, G.A., and Suflita, J.M., 1997, Confined subsurface microbial communities in Cretaceous rock: Nature, v. 386, p. 64–66, https://doi.org/10.1038/386064a0.

Leever, K.A., Gabrielsen, R.H., Faleide, J.I., and Braathen, A., 2011, A transpressional origin for the West Spitsbergen fold-and-thrust belt: Insight from analog modeling: Tectonics, v. 30, no. 2, TC2014, https://doi.org/10.1029/2010TC002753.

Lord, G.S., Mørk, M.B.E., Mørk, A., and Olaussen, S., 2019, Sedimentology and petrography of the Svenskøya Formation on Hopen, Svalbard: An analogue to sandstone reservoirs in the Realgrunnen Subgroup: Polar Research, v. 38, https://doi.org/10.33265/polar.v38.3523.

Lubrano-Lavadera, P., Senger, K., Lecomte, I., Mulrooney, M.J., and Kühn, D., 2019, Seismic modelling of metre-scale normal faults at a reservoir–cap rock interface in central Spitsbergen, Svalbard: Implications for CO_2 storage: Norwegian Journal of Geology, v. 99, no. 2, p. 329–347.

Machel, H.G., and Foght, J., 2000, Products and depth limits of microbial activity in petroliferous subsurface settings, in Riding, R.E., and Awramik, S.M., eds., Microbial Sediments: Berlin, Springer, p. 105–120, https://doi.org/10.1007/978-3-662-04036-2_13.

Maher, H., Senger, K., Braathen, A., Mulrooney, M.J., Smyrak-Sikora, A., Osmundsen, P.T., and Ogata, K., 2020, Mesozoic–Cenozoic regional stress field evolution in Svalbard: Tectonics, v. 39, https://doi.org/10.1029/2018TC005461.

Martinez-Ruiz, F., Paytan, A., Gonzalez-Muñoz, M.T., Jroundi, F., Abad, M.M., Lam, P.J., Bishop, J.K.B., Horner, T.J., Morton, P.L., and Kastner, M., 2019, Barite formation in the ocean: Origin of amorphous and crystalline precipitates: Chemical Geology, v. 511, p. 441–451, https://doi.org/10.1016/j.chemgeo.2018.09.011.

Mørk, M.B.E., 2013, Diagenesis and quartz cement distribution of low-permeability Upper Triassic–Middle Jurassic reservoir sandstones, Longyearbyen CO_2 lab well site in Svalbard, Norway: American Association of Petroleum Geologists Bulletin, v. 97, no. 4, p. 577–596, https://doi.org/10.1306/10031211193.

Mulrooney, M.J., Larsen, L., Stappen, J.V., Cnudde, V., Senger, K., Rismyhr, B., Braathen, A., Olaussen, S., Mørk, M.B.E., and Ogata, K., 2019, Fluid flow properties of the Wilhelmøya Subgroup, a potential unconventional CO_2 storage unit in central Spitsbergen: Norwegian Journal of Geology, v. 99, no. 2, p. 285–316, https://njg.geologi.no/vol-91-100/details/1/2188-2188.

Ogata, K., Senger, K., Braathen, A., and Tveranger, J., 2014, Fracture corridors as seal-bypass systems in siliciclastic reservoir–cap rock successions: Field-based insights from the Jurassic Entrada Formation (SE Utah, USA): Journal of Structural Geology, v. 66, p. 162–187, https://doi.org/10.1016/j.jsg.2014.05.005.

Olaussen, S., Senger, K., Braathen, A., Grundvåg, S.A., and Mørk, A., 2019, You learn as long as you drill: Research synthesis from the Longyearbyen CO_2 Laboratory, Svalbard, Norway: Norwegian Journal of Geology, v. 99, p. 157–187, https://doi.org/10.17850/njg008.

Parkes, R.J., Webster, G., Cragg, B.A., Weightman, A.J., Newberry, C.J., Ferdelman, T.G., Kallmeyer, J., Jørgensen, B.B., Aiello, I.W., and Fry, J.C., 2005, Deep sub-seafloor prokaryotes stimulated at interfaces over geological time: Nature, v. 436, p. 390–394, https://doi.org/10.1038/nature03796.

Parnell, J., Boyce, A.J., Hurst, A., Davidheiser-Kroll, B., and Ponicka, J., 2013, Long term geological record of a global deep subsurface microbial habitat in sand injection complexes: Scientific Reports, v. 3, 1828, p. 1–6, https://doi.org/10.1038/srep01828.

Paulsen, R.S., Birchall, T., Senger, K., and Grundvåg, S.-A., 2022, Seal characterization and integrity in uplifted basins: Insights from the northern Barents Shelf: Marine and Petroleum Geology, v. 139, https://doi.org/10.1016/j.marpetgeo.2022.105588.

Pernin, N., Feuilleaubois, L., Bird, T., and Reiser, C., 2022, Identifying and de-risking near-field opportunities through reliable pre-stack broadband attributes: Examples from the Paleocene North Sea (UK–Norway) injectites play, in Patruno, S., et al., eds., Cross-Border Themes in Petroleum Geology I: The North Sea: Geological Society, London, Special Publication 494, p. 445–459, https://doi.org/10.1144/SP494-2019-11.

Peterson, G.L., 1968, Flow structures in sandstone dikes: Sedimentary Geology, v. 2, no. 3, p. 177–190, https://doi.org/10.1016/0037-0738(68)90024-9.

Quigley, M.C., Bastin, S., and Bradley, B.A., 2013, Recurrent liquefaction in Christchurch, New Zealand, during the Canterbury earthquake sequence: Geology, v. 41, no. 4, p. 419–422, https://doi.org/10.1130/G33944.1.

Rismyhr, B., Bjærke, T., Olaussen, S., Mulrooney, M.J., and Senger, K., 2019, Facies, palynostratigraphy and sequence stratigraphy of the Wilhelmøya Subgroup (Upper Triassic–Middle

Jurassic) in western central Spitsbergen, Svalbard: Norwegian Journal of Geology, v. 99, p. 35–64, https://doi.org/10.17850/njg001.

Ross, J.A., Peakall, J., and Keevil, G.M., 2011, An integrated model of extrusive sand injectites in cohesionless sediments: Sedimentology, v. 58, no. 7, p. 1693–1715, https://doi.org/10.1111/j.1365-3091.2011.01230.x.

Ross, J.A., Peakall, J., and Keevil, G.M., 2014, Facies and flow regimes of sandstone-hosted columnar intrusions: Insights from the pipes of Kodachrome Basin State Park: Sedimentology, v. 61, no. 6, p. 1764–1792, https://doi.org/10.1111/sed.12115.

Ross, P.S., and White, J.D.L., 2005, Unusually large clastic dykes formed by elutriation of a poorly sorted, coarser-grained source: Journal of the Geological Society, v. 162, p. 579–582, https://doi.org/10.1144/0016-764904-127.

Scott, A., Hurst, A., and Vigorito, M., 2013, Outcrop-based reservoir characterization of a kilometer-scale sand-injectite complex: American Association of Petroleum Geologists Bulletin, v. 97, no. 2, p. 309–343, https://doi.org/10.1306/05141211184.

Senger, K., Tveranger, J., Ogata, K., Braathen, A., and Planke, S., 2014, Late Mesozoic magmatism in Svalbard: A review: Earth-Science Reviews, v. 139, p. 123–144, https://doi.org/10.1016/j.earscirev.2014.09.002.

Senger, K., Tveranger, J., Braathen, A., Olaussen, S., Ogata, K., and Larsen, L., 2015, CO_2 storage resource estimates in unconventional reservoirs: Insights from a pilot-sized storage site in Svalbard, Arctic Norway: Environmental Earth Sciences, v. 73, no. 8, p. 3987–4009, https://doi.org/10.1007/s12665-014-3684-9.

Senger, K., Millett, J., Planke, S., Ogata, K., Eide, C.H., Festøy, M., Galland, O., and Jerram, D.A., 2017, Effects of igneous intrusions on the petroleum system: A review: First Break, v. 35, no. 6, https://doi.org/10.3997/1365-2397.2017011.

Steel, R., Gjelberg, J., Helland-Hansen, W., Kleinspehn, K., Nøttvedt, A., and Rye-Larsen, M., 1985, The Tertiary strike-slip basins and orogenic belt of Spitsbergen, in Biddle, K.T., and Christie-Blick, N., eds., Strike-Slip Deformation, Basin Formation, and Sedimentation: Society of Economic Paleontologists and Mineralogists (SEPM) Special Publication 37, p. 339–359, https://www.jsg.utexas.edu/svalex/files/Steel_etal_1985.pdf.

Sultan, N., Plaza-Faverola, A., Vadakkepuliyambatta, S., Buenz, S., and Knies, J., 2020, Impact of tides and sea-level on deep-sea Arctic methane emissions: Nature Communications, v. 11, 5087, https://doi.org/10.1038/s41467-020-18899-3.

Taylor, B.J., 1982, Sedimentary dykes, pipes and related structures in the Mesozoic sediments of south-eastern Alexander Island: British Antarctic Survey Bulletin, v. 51, p. 1–42, http://nora.nerc.ac.uk/id/eprint/524505.

Templeton, G., McInally, A., Melvin, A., and Batchelor, T., 2006, Comparison of Leadon and Gryphon fields sand injectites—Occurrence and performance, in 68th European Association of Geoscientists and Engineers (EAGE) Conference and Exhibition incorporating SPE EUROPEC 2006, https://doi.org/10.3997/2214-4609.201402261.

Tsikalas, F., Dypvik, H., and Smelror, M., eds., 2010, The Mjølnir Impact Event and its Consequences (1st edition): Berlin, Springer, Impact Studies, p. 139–174.

Wierzbowski, A., and Ziembińska-Tworzydło, M., 1984, Paleocene clastic dyke at Janusfjellet, Spitsbergen: Polish Polar Research, v. 5, no. 3–4, p. 331–335.

Worsley, D., 2008, The post-Caledonian development of Svalbard and the western Barents Sea: Polar Research, v. 27, no. 3, p. 298–317, https://doi.org/10.1111/j.1751-8369.2008.00085.x.